Carbonate facies evolution, bio- and carbon isotope stratigraphy through the Ludfordian (Silurian) on the shelf of Baltica (Lithuania)

Anna Cichon-Pupienis, Andrej Spiridonov, Ieva Kaminskaitė-Baranauskienė, Robertas Stankevič, Andrius Garbaras & Sigitas Radzevičius

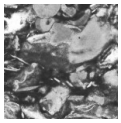

A 95-metre-long subsurface stratigraphical interval of the late Ludlow (Silurian) representing shelf deposits of the Baltica palaeocontinent (Lithuania) was investigated in terms of bio-, carbon isotope stratigraphy as well as litho- and microfacies. The conodont biostratigraphic data confirm the Ludfordian age (*Kockelella variabilis* Zone to *Jeppssonia crispa* Zone) of the succession. The deposits recorded a positive stable carbon isotope $\delta^{13}C_{carb}$ excursion referred to as the Mid-Ludfordian Carbon Isotope Excursion beginning in the uppermost *Polygnathoides siluricus* Zone and fully developed throughout the *P. latialata–Jeppssonia snajdri* Interval Biozone. The lithologically variable succession reflects a general shallowing-upward trend encompassing a broad range of different depositional environments and palaeowater depths. In vertical succession, deep-shelf argillaceous-marly sediments gradually pass into shallow-water carbonates, including reef-related lithologies, and extend into peritidal environments. Such a transition is indicative of prolonged progradational conditions. Furthermore, the sedimentological record provides evidence for short-term fluctuations in sea level that could be of glacio-eustatic origin. Microbial carbonates occur in significant abundance as oncoids within beds, which recorded the highest amplitude of $\delta^{13}C_{carb,}$ reaching a maximum value of +7.5‰. • Key words: carbonates, depositional environment, Silurian Baltic Basin, Ludlow, C-isotope excursion.

Cichon-Pupienis, A., Spiridonov, A., Kaminskaitė-Baranauskienė, I., Stankevič, R., Garbaras, A. & Radzevičius, S. 2025. Carbonate facies evolution, bio- and carbon isotope stratigraphy through the Ludfordian (Silurian) on the shelf of Baltica (Lithuania). *Bulletin of Geosciences 100*(*X*), xxx–xxx (19 figures, 3 electronic appendices). Czech Geological Survey, Prague. ISSN 1214-1119. Manuscript received March 24, 2025; accepted in revised form September 9, 2025; published online November 9, 2025; issued Xxxxxxxx XX, 2025.

Anna Cichon-Pupienis (corresponding author), Laboratory of Bedrock Geology, State Scientific Research Institute Nature Research Centre, Akademijos str. 2, 08412 Vilnius, Lithuania; anna.cichon-pupienis@gamtc.lt • Andrej Spiridonov, Ieva Kaminskaitė-Baranauskienė, Robertas Stankevič & Sigitas Radzevičius, Department of Geology and Mineralogy, Vilnius University, M. K. Čiurlionio 21/27, 03101 Vilnius, Lithuania • Andrius Garbaras, Department of Nuclear Research, Center for Physical Sciences and Technology, 10221 Vilnius, Lithuania

In the last couple of decades, the Silurian period has attracted scientific attention due to the presence of several distinct positive carbon isotope excursions recorded in both deep and shallow marine environments, as well as the co-occurrence of faunal extinctions (see summary in Calner 2008, Munnecke *et al*. 2010). The carbon isotope excursion (CIE) in Ludfordian sediments is regarded as the largest of the Silurian and Phanerozoic and so far has been documented across different palaeocontinents: Gondwana (Andrew *et al*. 1994), peri-Gondwana (Lehnert *et al*. 2003, 2007a, b; Vecoli *et al*. 2009; Frýda & Manda 2013; Gocke *et al*. 2013; Frýda *et al.* 2021a, b), Avalonia (Loydell & Frýda 2011), Laurentia (Saltzman 2001; Barrick *et al*. 2010, 2011; Strauss *et al*. 2020), Baltica (Samtleben *et al*. 1996; Wenzel & Joachimski 1996; Martma *et al*. 2005; Kozłowski & Munnecke 2010; Kozłowski & Sobień 2012; Kozłowski 2015, 2020; Bowman *et al*. 2020).

The Ludfordian marine faunal crisis affected various benthic and pelagic communities in a stepwise and asynchronous manner (see discussions in Jeppsson *et al.* 2012, Mergl *et al.* 2018, Frýda *et al.* 2021b, Tonarová *et al.* 2025) with the most notable changes observed in conodonts in shallow shelf facies (the Lau Event) and graptolites in deep-water facies (the *Kozlowskii* Event, *e.g.* Calner 2008, Jeppsson *et al.* 2012). There is an ongoing debate on the mechanism responsible for the changes in the global carbon cycle, mirrored in the carbon isotope excursion, and close in-time faunal biocrises. Climatic perturbations have been suggested as the most probable cause; however, the overall driving mechanism is likely to be considerably more complex, involving interdependent and synchronous palaeoceanographic processes (summary in Munnecke *et al*. 2010). Indeed, the observed changes in the oxygen isotope compositions of brachiopod calcite

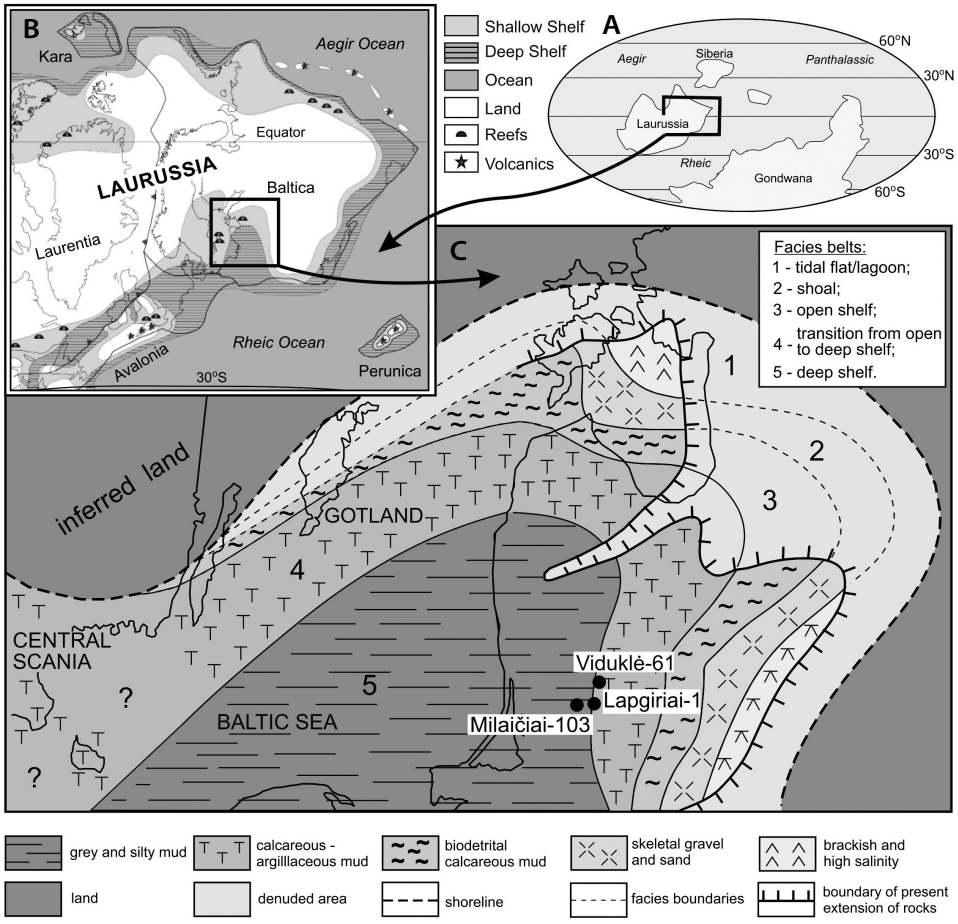

Figure 1. The study area. • A – location of Silurian palaeocontinents (Torsvik & Cocks 2013). • B – the mid–Silurian palaeogeographical map of Laurussia (Cocks & Torsvik 2005). • C – facies distribution after Bassett *et al*. (1989) with the location of the studied boreholes.

and conodont phosphate at different palaeocontinents were interpreted in terms of palaeotemperature shifts that coincide with the Mid-Ludfordian CIE, thereby suggesting a global cooling (glaciation) episode (see Frýda *et al.* 2021b and references therein).

Climate and tectonic perturbations are strong predictors of the global biodiversity patterns and their spatial structures over time scales of millions to tens of millions of years (Eichenseer *et al*. 2019, Mathes *et al*. 2021, Spiridonov & Lovejoy 2022, Spiridonov *et al*. 2022, Lovejoy & Spiridonov 2024). The distribution of conodont species and changes in their communities form the basis for distinguishing global climatically and oceanographically forced Silurian episodes and events (Jeppsson 1998; Jeppsson & Aldridge 2000; Calner 2008; Cramer *et al*. 2011; Sadler 2012; Radzevičius *et al*. 2014c, 2016; Jarochowska *et al*. 2016; Spiridonov *et al*. 2017a, 2020b; Melchin *et al*. 2020). More recently, changes in the abundance of conodonts (Girard & Renaud 2007; Spiridonov *et al*. 2015, 2016; Spiridonov 2017) and acritarchs (Spiridonov *et al*. 2017c, Stankevič *et al.* 2024) have been recognised as an important variable in describing community composition, showing an association between abundance explosions and collapses and intercalating oceanic/biospheric states (Stricanne *et al*. 2004, Whittingham *et al*. 2022). Here, the stratigraphic distributions, quantitative assemblage compositions, and conodont abundance patterns observed in the Lapgiriai-1 core section are reported. These data sets were employed for quantitative stratigraphical correlation using cross-recurrence plots (Marwan *et al*. 2002, 2007; Spiridonov 2017) of conodont assemblage compositions. This approach enabled the quantification of the uncertainties of the correlations and the identification of possible causes of uncertainty related to dramatic changes in conodont abundance.

Past climatic forces and associated changes in global sea-level, as well as regional tectonic settings/events, have influenced sedimentary conditions, which in turn are archived in the sedimentary record. In certain locations, more detailed sedimentological studies of the Ludfordian sections in Baltica and peri-Gondwana demonstrated distinct changes in lithology, commonly implying a shallowing of environmental conditions caused by sea-level fall accompanied by a positive shift in the carbon isotope curve (Kozłowski 2003, Johnson 2006, Lehnert *et al.* 2007a, Eriksson & Calner 2008, Kozłowski & Munnecke 2010, Kozłowski & Sobień 2012, Gocke *et al*. 2013). The Silurian lateral facies pattern, which developed on the

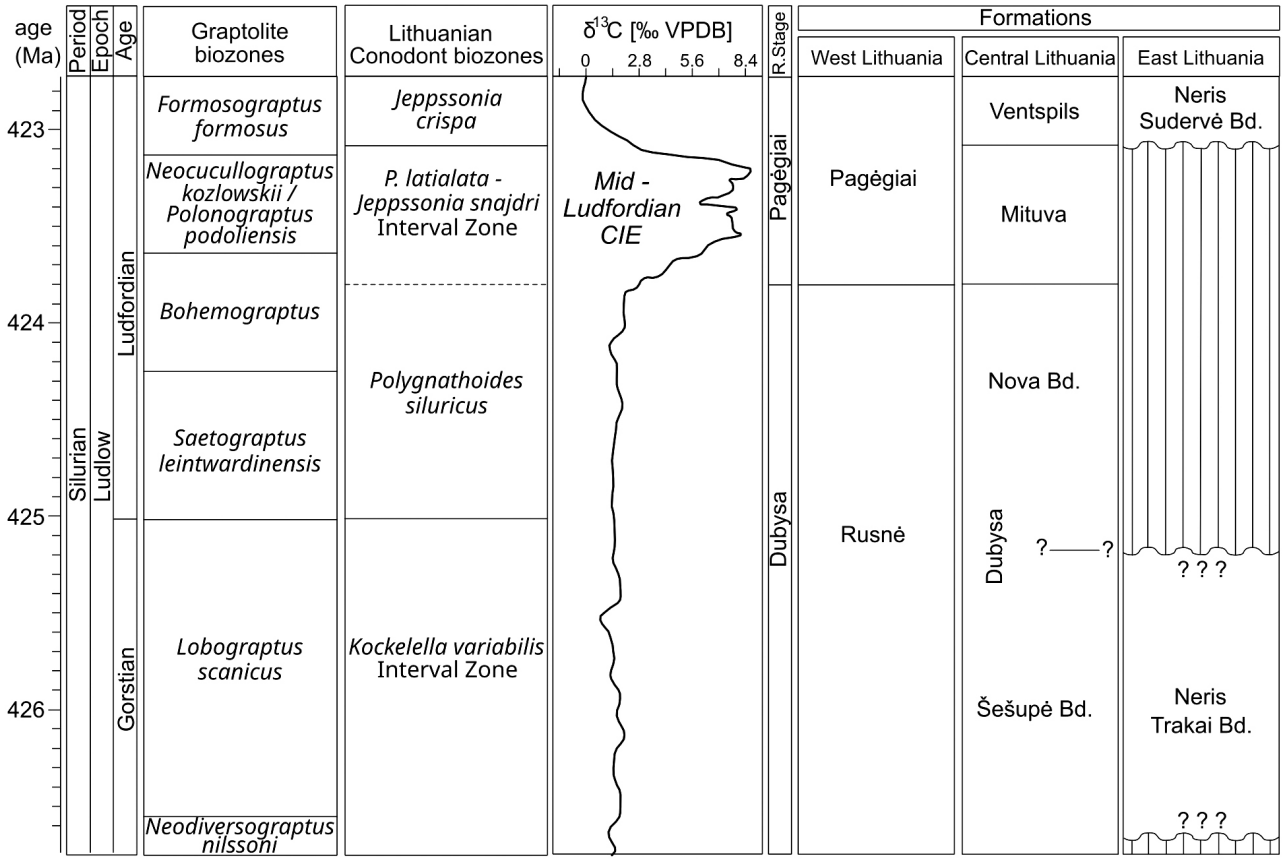

Figure 2. Correlation of Silurian timescale with graptolite biozonation and the generalized $\delta^{13}C$ curve (Melchin *et al*. 2020) with Lithuanian conodont Zones (Spiridonov *et al*. 2020a), regional stages (Paškevičius *et al*. 1994) and associated formations (East Lithuania based on Želvys *et al*. 2022).

SW margin of the Baltica palaeocontinent, is commonly presented as facies belts arranged linearly parallel to the basin edge (Bassett *et al*. 1989, Klaamann & Einasto 1982, Baarli *et al*. 2003). However, the nature and geometry of the carbonate shelf and the character of stromatoporoid structures, with a potential to form a barrier separating an outer shelf from an inner shelf, remain a matter of debate, and were explored in more detail by Samtleben *et al*. 2000; Bičkauskas & Molenaar 2008a, b; Skompski *et al*. 2008; Łuczyński *et al*. 2009; and Kaminskas *et al*. 2015.

In this paper, new data is presented from the Lapgiriai-1 borehole, palaeogeographically situated on the shelf of the Baltica palaeocontinent within tropical latitudes in late Silurian times (Fig. 1). In order to develop a more in-depth understanding of the palaeoenvironmental evolution that prevailed in the eastern part of the Baltic Basin throughout the Ludfordian, this study investigates the temporal sedimentary facies change in relation to shifts in carbon isotope curve and conodont biostratigraphic data within a core section. Despite the fact that two other core sections of Ludlow from Lithuania (Viduklė-61 and Milaičiai-103, Fig. 1) were examined in terms of bio- and chemostratigraphy, no detailed facies descriptions have been provided (Martma *et al*. 2005, Spiridonov *et al*. 2017b). The location of the studied section within a relatively shallow part of the basin, which was exposed to sea-level fluctuations, enabled the detection of changes in sedimentation that are difficult or impossible to observe in the deep-water shelf sections. Moreover, this provides an opportunity to compare the facies record with sections from other localities, especially comparable settings within the basin, such as those observed on Gotland. The integration of new data will facilitate a more comprehensive reconstruction of the Silurian facies patterns on the shelf of Baltica. This will, in turn, allow for a better understanding of past depositional environments and basin evolution, offering insights into the local or global factors that determined deposition and potentially triggered biotic changes.

Geological setting

All samples were collected from a nearly complete core section of the Lapgiriai-1 borehole located in Central Lithuania (Fig. 1). In terms of palaeogeography, the borehole was situated on the south-western shelf of the Baltica palaeocontinent, which collided with Laurentia during the Silurian (Fig. 1A, B; Torsvik & Cocks 2013),

consequently forming the Laurussia palaeocontinent. In late Silurian times, Laurussia, and thus Baltica, was positioned within the tropical belt (Fig. 1A, B). The Caledonian convergence and collision of continental plates led to foreland flexure of the western margin of Baltica, and consequently, subsidence, deepening of the basin, and sediment infill enhanced in the late Silurian (Lazauskienė *et al*. 2002). The configuration of the basin on the SW margin of Baltica produced a distinct facies arrangement parallel to the basin margin, extending from the Baltic Sea region to Ukraine (Fig. 1C). Shallow-water carbonate sedimentation was characteristic of the north-east margin, while deep-water siliciclastic mudstone deposition prevailed in the southwestern part of the basin (Fig. 1C; Klaamann & Einasto 1982, Einasto *et al*. 1986, Bassett *et al*. 1989, Baarli *et al*. 2003 and references therein). In Lithuania, a clear transition is observed from deep-shelf claystones in the west to shallow-water carbonates toward Eastern Lithuania (Fig. 1C). In the studied area, the entire Silurian succession reaches around 550 m in thickness (Paškevičius 1997), but the cored interval is 95 m and generally encompasses the Ludfordian section (Fig. 2, 3).

The Ludlow series in Lithuania is divided into two regional stages (R.S.): the Dubysa and Pagėgiai (Fig. 2). The Dubysa R.S. is of greater duration than the Gorstian global stage, *i.e.* it refers to the *Kockelella variabilis* conodont Zone, and encompasses a portion of the Ludfordian assigned to *Polygnathoides siluricus* Zone. In Western Lithuania, Dubysa R.S. is represented by Rusnė Fm., which is composed of dark-grey to black siliciclastic mudstones with calcareous concretions and thin interlayers of clayey fine-grained limestones. Towards the east, in Central Lithuania, the dominant muddy lithologies are gradually replaced by greenish-grey marls, nodular fine-grained limestones, and fine-grained to organogenic-detrital limestones of the Šešupė and Nova beds. Pagėgiai R. S. corresponds to *P. latialata–Jeppssonia snajdri* Interval Biozone and *Jeppssonia crispa* conodont Zones and is represented by Pagėgiai Fm. in West Lithuania that grades into Mituva and Ventspils Fms in Central Lithuania. Pagėgiai Fm. overlies Rusnė Fm. in West Lithuania, where it is dominated by greenish-grey siliciclastic mudstones with calcareous concretions, marls, and fine-grained and detrital limestone interlayers. The lithology of the Mituva Fm. is highly variable and generally developed as greenish-grey calcareous mudstone-marls with fine-grained limestone interlayers and nodules, wavy-bedded to nodular limestones, oncolitic limestones, organogenic-detrital limestones, and laminated dolomitic marls with fine-grained limestones. The Ventspils Fm., which overlies the Mituva Fm., is characterized by the prevalence of nodular to wavy-bedded fine-grained and organogenic-detrital limestones with interlayers of dark-grey to black marls. In East Lithuania, the Ludlow succession is significantly reduced, and only the Neris Fm. is recognized (Fig. 2). This formation is subdivided into the Trakai (corresponding to *K. variabilis* Zone*)* and Sudervė beds (*J. crispa* Zone, Fig. 2). It is suspected that there is a stratigraphic gap between the two, spanning the *P. siluricus Zone* and *P. latialata–Jeppssonia snajdri* Interval Biozone (Spiridonov *et al*. 2020a, Želvys *et al*. 2022). The Trakai beds are predominantly characterized by grey massive dolomites with interlayers of marls and nodular dolomitic limestones, while the Sudervė beds are composed of grey nodular or detrital limestones and dolomites with lenses of grey to black marls.

Material and methods

The cored interval of the Lapgiriai-1 borehole is 95 m in length and it is stored at the Vievis core facility of the Lithuanian Geological Survey (Fig. 3). In total, 95 samples were collected at approximately 1 m intervals within the depth interval between 1129 and 1026 m. These samples were analysed for stable isotope composition, conodont abundance, and taxonomic compositional changes. Over 50 samples were collected for microfacies analysis, while 3 additional samples from oncolitic beds were obtained from the Viduklė-61 borehole (Fig. 1, 3). Additionally, a natural gamma-ray (GR) log from the borehole, archived at the Lithuanian Geological Survey, was utilized.

Facies analysis. – The identification of facies was based on the analysis of core material and microfacies, with attention paid to changes in lithology, texture, sedimentary structures, grain characteristics, and fossil assemblage diversity. Standard petrographic thin section analysis was conducted using a Nikon Eclipse LV100N POL microscope, equipped with NIS-Elements D software. Thin-section images were also produced by scanning the thin sections using Microvisioneer manual WSI software. Selected thin sections were further examined using scanning electron microscopy (SEM) facilities at the State Scientific Research Institute Nature Research Centre in Vilnius. The characterization of facies types follows the Facies Zones (FZ) and associated Standard Microfacies Types (SMF) proposed by Wilson (1975), as modified by Flügel (2010), and includes Ramp Microfacies Types (RMF) summarized in Flügel (2010).

Figure 3. Generalized lithology and conodont stratigraphy of the Lapgiriai-1 drill core with bulk carbon and oxygen isotope records, and proposed sequence stratigraphy interpretation. Samples of thin sections are indicated as black arrows.

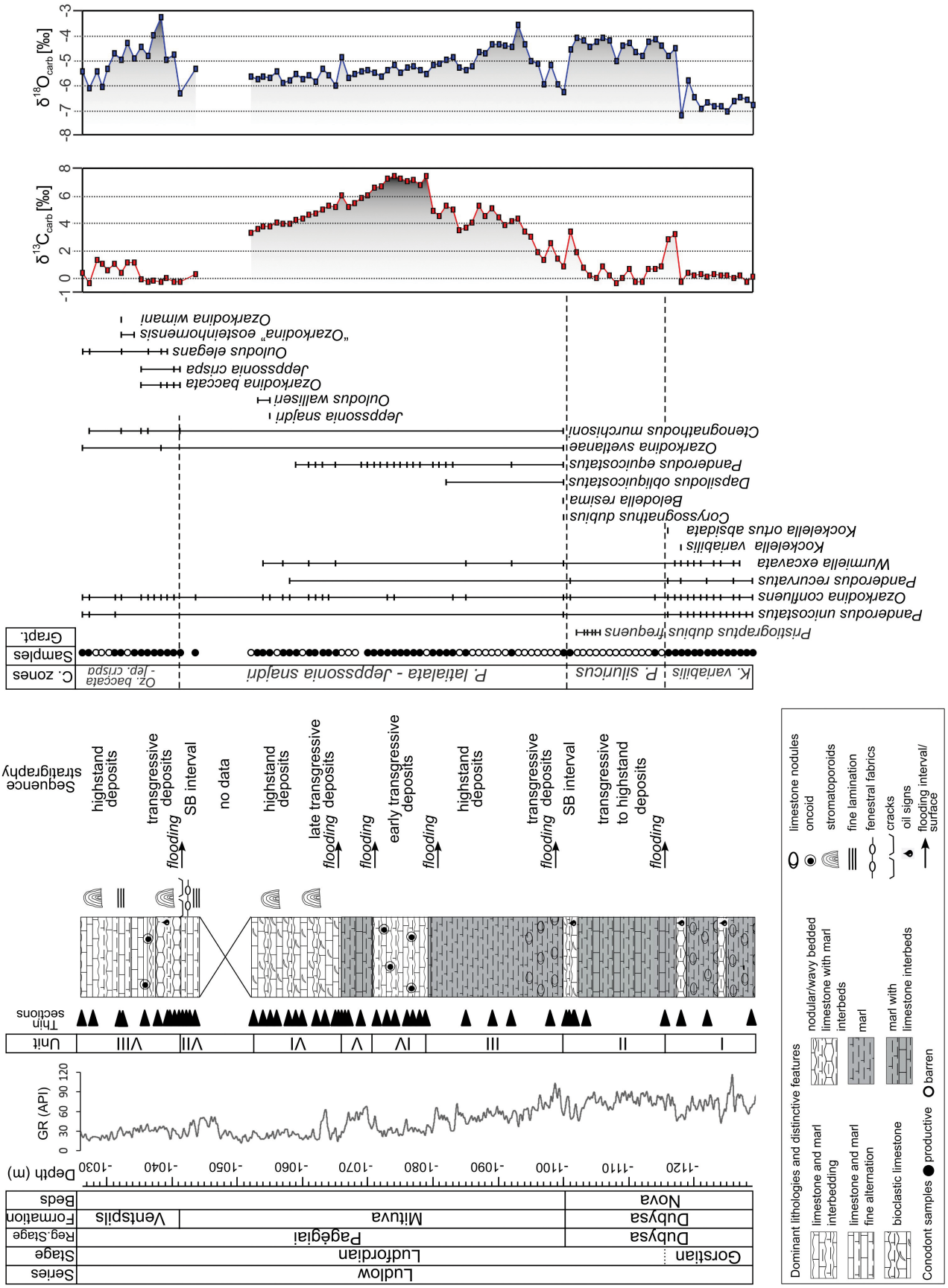
δ18Ocarb [‰]
δ13Ccarb [‰]
K. variabilis
P. siluricus
P. latialata - Jeppssonia snajdri
Oz. baccata - Jep. crispa
C. zones
Samples
Grapt.
Pristiograptus dubius frequens
Panderodus unicostatus
Ozarkodina confluens
Panderodus recurvatus
Wurmiella excavata
Kockelella variabilis
Kockelella ortus absidata
Coryssognathus dubius
Belodella resima
Dapsilodus obliquicostatus
Panderodus equicostatus
Ozarkodina svetlanae
Ctenognathodus murchisoni
Jeppssonia snajdri
Oulodus walliseri
Ozarkodina baccata
Jeppssonia crispa
Oulodus elegans
"Ozarkodina" eosteinhornensis
Ozarkodina wimani
Series
Stage
Reg.Stage
Formation
Beds
Ludlow
Gorstian
Ludfordian
Dubysa
Pagėgiai
Mituva
Ventspils
Nova
Depth (m)
GR (API)
Unit
Thin sections
highstand deposits
transgressive deposits
flooding
SB interval
no data
late transgressive deposits
early transgressive deposits
to highstand deposits
Sequence stratigraphy
Dominant lithologies and distinctive features
limestone and marl interbedding
limestone and marl fine alternation
bioclastic limestone
nodular/wavy bedded limestone with marl interbeds
marl
marl with limestone interbeds
limestone nodules
oncoid
stromatoporoids
fine lamination
fenestral fabrics
cracks
oil signs
flooding interval/ surface
Conodont samples ● productive ○ barren

Conodont data. – Conodont samples were prepared using standard procedures, involving the dissolution of carbonate rocks with buffered formic acid (Jeppsson & Anehus 1995, Radzevičius *et al*. 2014b). The resulting residues were sieved into fractions to facilitate manual picking, and all samples were exhaustively examined under a binocular microscope for conodont elements. In total, 95 samples were analyzed for conodont content, spanning the Ludlow Epoch; 47 samples were productive, while the rest were barren (Fig. 3). All conodont samples are archived at the Museum of Geology in Vilnius University, Department of Geology and Mineralogy.

Recurrence and cross-recurrence plots and stratigraphic correlation. – Recurrence plots and recurrence quantification analysis are powerful nonlinear techniques, used in determining dynamic characteristics of complex, noisy, non-linear, and often non-stationary time series (Marwan & Webber 2015, Webber & Marwan 2015), including palaeoecological and stratigraphic records (Spiridonov *et al*. 2019, Trauth *et al*. 2019, Marwan *et al*. 2021, Spiridonov *et al*. 2021, Stankevič *et al*. 2024). The recurrence plots compare all states of a system to all other states, which can be quantitative or categorical values of a time series, or alternatively, delay embedded "states" of the system. Essentially, a recurrence plot is a binary matrix of "similar" (black in the plot) and "dissimilar" (white in the plot) values between observations of the same time series (or other ordered series, such as stratigraphic series), in which case we have a square matrix. The threshold for determining similarity is task-specific and depends on the length and statistical properties of the time series. In the case of non-stationary or wandering time series (*i.e.* those resembling a random walk), the threshold is typically adjusted to yield a recurrence rate (RR) of 20–30% (Spiridonov *et al*. 2020a, b). When comparing two observational series of different lengths (in number of observations), a rectangular matrix of cross-similarities is generated. The binary-filtered matrix, consisting of similar points (black) and dissimilar points (white), is termed a cross-recurrence plot (Marwan *et al*. 2002). This kind of matrix can be used for the exploration of correlated evolution of two multivariate or univariate palaeoecological time series, and even used as a tool for graphical biostratigraphical correlation (Spiridonov 2017).

In this study, the Morisita-Horn index was used as the dissimilarity metric, which takes into account both species presence/absence and their relative abundances (Horn 1966). Samples barren of conodonts were assigned a similarity value of "0", a conservative approach that avoids inflating recurrence without evidence of positive similarity. This approach has been used in several studies, revealing interactions between biotic and abiotic factors influencing Silurian bioevents (Radzevičius *et al*. 2016, Spiridonov *et al*. 2020b). Moreover, the experiments using different metrics generally show very similar results, with only minor nuances to the outlined approach (Spiridonov *et al*. 2020b).

Cross-recurrence plots were used to generate a graphic correlation of conodont communities between the Lapgiriai-1 section and the stratigraphically well-resolved Viduklė-61 section, which is considered a reference standard for the Baltic Basin (Radzevičius *et al*. 2014a, b, 2017; Venckutė-Aleksienė *et al*. 2016; Spiridonov *et al*. 2020a). Conodont data from the Viduklė-61 section were obtained from Spiridonov *et al*. (2020a). The graphical correlation was performed using the dynamical time warping algorithm (DTW), which identifies minimal cost paths in the distance matrix (here, among similar or black values of a cross-recurrence plot), which connects the starting and ending corners of the matrix (Hladil *et al*. 2010, Spiridonov *et al*. 2020a). This isotonic (monotonously increasing) synchronization path is equivalent to a correlation line between two sections in graphical stratigraphic correlation (Sadler 2004*,* Sadler *et al.* 2014, Spiridonov 2017). To assess uncertainty, the DTW algorithm was applied across cross-recurrence plots with different recurrence rates (RRs). The same DTW algorithm as in Spiridonov *et al*. (2020a) was used here, but with probable correlation lines estimated at different RR. The recurrence rates were set to the given thresholds (*e.g.* RR = 10, 20, 30%) by automatically varying the filtering threshold similarity for the recurrence "ε". Standard deviations in the correlation line position, calculated relative to depth in the Viduklė-61 core, served as a measure of uncertainty, benchmarked against well-established conodont zones in this deep-water section.

Stable isotopes. – For the purposes of stable isotope analysis, 95 whole-rock samples of vein-free marlstones and

Figure 4. Characteristic facies types of the calcareous mudstone–marl section. • A – marl with lime mudstone nodule (lighter colour) and bioclastic debris. Fracture is filled with blocky sparry cement (unit I, 1129.0 m). • B, B1 – hand specimen (1115.4 m) and corresponding thin sections (B2, 3) showing boundary separating two units I and II with inferred hardground – the surface is marked by black impregnation (probably Fe/Mn crust). Note differences in facies of unit I (lower part, *K. variabilis* Zone) and unit II (upper part– inferred *P. siluricus* Zone); B2 – close-up view (black square in B1) of bioclasts affected by intense microboring at the units' boundary; B3 – thin section exhibiting a high degree of pyritization (bright colour) at the boundary (in reflected light). • C – the contact between the plane thin limestone bed (upper part) and the underlying marl (unit II, 1103.4 m). Limestone shows a crystalline texture. • D, E – marl, rich in bioclasts representing fossiliferous intervals within unit III (1085.0 and 1092.0 m). The section is patchily dolomitized. Note the geopetal fabric in a shell filled with matrix sediment and sparry calcite (E).

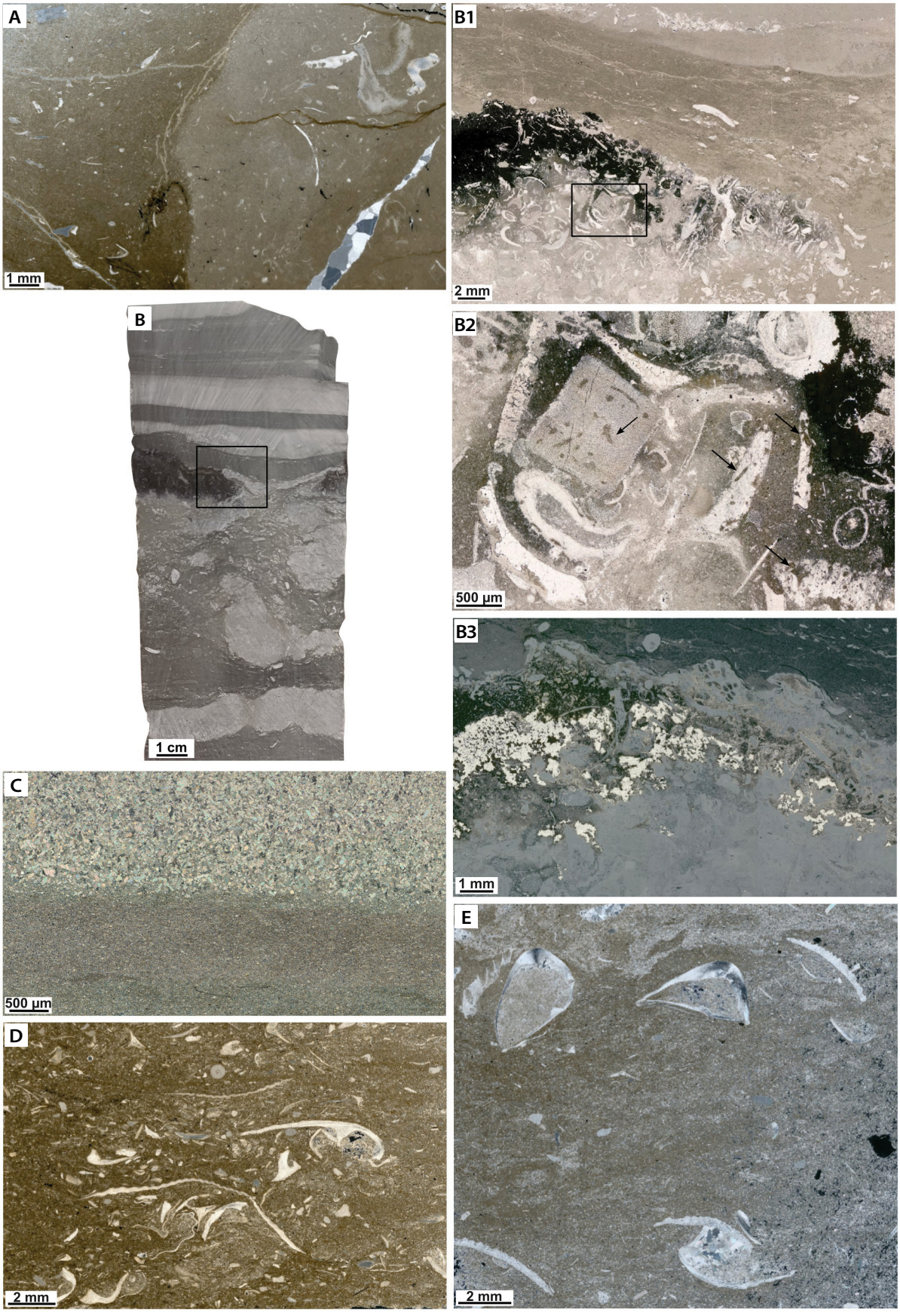
A
1 mm
B1
2 mm
B
1 cm
B2
500 µm
B3
1 mm
C
500 µm
D
2 mm
E
2 mm

limestones were selected and ground into powder. The analysis of stable carbon and oxygen isotope composition was conducted at the Nuclear Research Department of the State Research Institute Center for Physical Sciences and Technology, Vilnius, Lithuania. Sample powder was loaded into 10 mL Labco Exetainer vials, flushed with helium, treated with 99.99% H_3PO_4 at 50 °C for 10 h, before being analysed using a Thermo Gasbench II system combined with a Thermo Delta V isotope ratio mass spectro-meter. Isotopic values for carbon and oxygen are reported per mil (‰), relative to the Vienna PeeDee Belemnite (VPDB) standard and calibrated using certified international standards IAEA-CO-8 and IAEA-CO-9. The precision of the isotope analyses is ± 0.10‰ ($\delta^{13}C_{carb}$), ± 0.15‰ ($\delta^{18}O$). The accuracy of the analyses is on the order of $\sigma = 0.10$‰.

The regional thermal maturity trends within the lower part of the Palaeozoic succession indicate a low degree of thermal alteration of organic matter in the studied area, as reflected by the low Colour Alteration Index (CAI 1) of conodont specimens (Nehring-Lefeld *et al*. 1997, Zdanaviciutė & Lazauskienė 2007). This is supported by the good preservation of conodont specimens, which render the rocks suitable for stable isotope studies.

Results

Facies descriptions

The investigated core is subdivided into eight distinct lithological units (Fig. 3) characterized by specific facies or facies associations indicating different depositional environments.

Units I, II and III

Units I, II and III are composed of greenish-dark grey calcareous mudstones/marls with subordinate limestone beds (Fig. 3). All three sections contain similar fossil assemblages, *i.e.* unevenly distributed, poorly-sorted bioclastic debris such as typically disarticulated shells or fragments of brachiopods, echinoderms, trilobites, and tiny ostracods, sometimes affected by borings (Fig. 4A). Nevertheless, graptolites were found in the upper part of unit II (Fig. 3). The bioclast content is the highest in Unit III and generally increases towards the upper portion of this section. The overall carbonate content increases in relation to the detrital terrigenous material upwards in the section, as reflected by decreasing values of rock natural gamma-ray (Fig. 3, GR). Undisturbed shells often display internal geopetal fabrics, filled with sediment and/or sparite (Fig. 4E). Dispersed fine pyrite and its clusters, and small nodules (possibly associated with organic components) are observed. Filamentous organic particles often exhibit parallel orientation to bedding, likely resulting from compaction. Units, especially III in particular, are affected by dolomitization (Fig. 4D, E). Carbonate nodules composed of argillaceous bioclastic lime mudstone (Fig. 4A), up to a few cm in diameter, and often grading into layers, are abundant, especially in Unit I and in the lower part of Unit III, but become more diffuse in the rest of Unit III. Unit II is particularly characterized by distinct, relatively uniformly distributed one to a few centimetre-thick horizontal elongated limestone nodules/beds (Fig. 4B). Microfacies analysis of these beds/nodules revealed a crystalline texture (Fig. 4C). A distinct boundary exists between units I and II at around 1116 m depth (Fig. 4B). This horizon is marked by an erosional relief and probably Mn/Fe impregnation, pyritization and reworked bioclasts hosted within the uppermost Unit I (Fig. 4B1, B2, B3).

The limestone beds embedded within Unit I (Fig. 3) show nodular/wavy-bedded fabrics with marlstone interlayers. Microfacies analysis indicates bioclastic wackestone-packstone texture with reworked, poorly sorted skeletal fragments of frequent brachiopod, ostracod, echinoderm, trilobite, and less common gastropod (Fig. 5A). The limestone shows signs of recrystallization, revealing suspicious peloidal fabrics.

In the uppermost part of Unit II, a 2-metre-thick limestone occurs, marked by abrupt facies change. It is composed of wavy-bedded fine-grained limestone, intervening with thin beds of marlstone and bioclastic limestone. The interval is patchily, but intensely stained with oil (Fig. 5B, C). The bioclastic limestones, with beds up to dm thick, are classified as skeletal packstones to grainstones (Fig. 5B, C). These beds are rich in diverse reworked bioclastic material, ranging from poorly to moderately sorted assemblages of echinoderms, fragments of corals, brachiopods, trilobites, ostracods, or alternatively, with a predominant skeletal group (crinoidal). In the grainstone, pore spaces are frequently filled with syntaxial overgrowths or sparry calcite cement. In the packstone, larger fossil fragments show pressure solution features at their contacts.

Figure 5. Texture variability in limestone beds embedded within a marly complex. • A – bioclastic wackestone–packstone (unit I, 1118.3 m) of argillaceous limestone nodule and surrounding marl, both rich in various poorly sorted fossils. • B – bioclastic packstone with reworked skeletal grains. Some echinoderm particles are affected by microborings (unit II, 1101.4 m). • C – bioclastic grainstone with moderately well–sorted skeletal grains and cement filling interparticle space (unit II, 1101.8 m). All samples are partly oil-stained (yellowish-brownish colour).

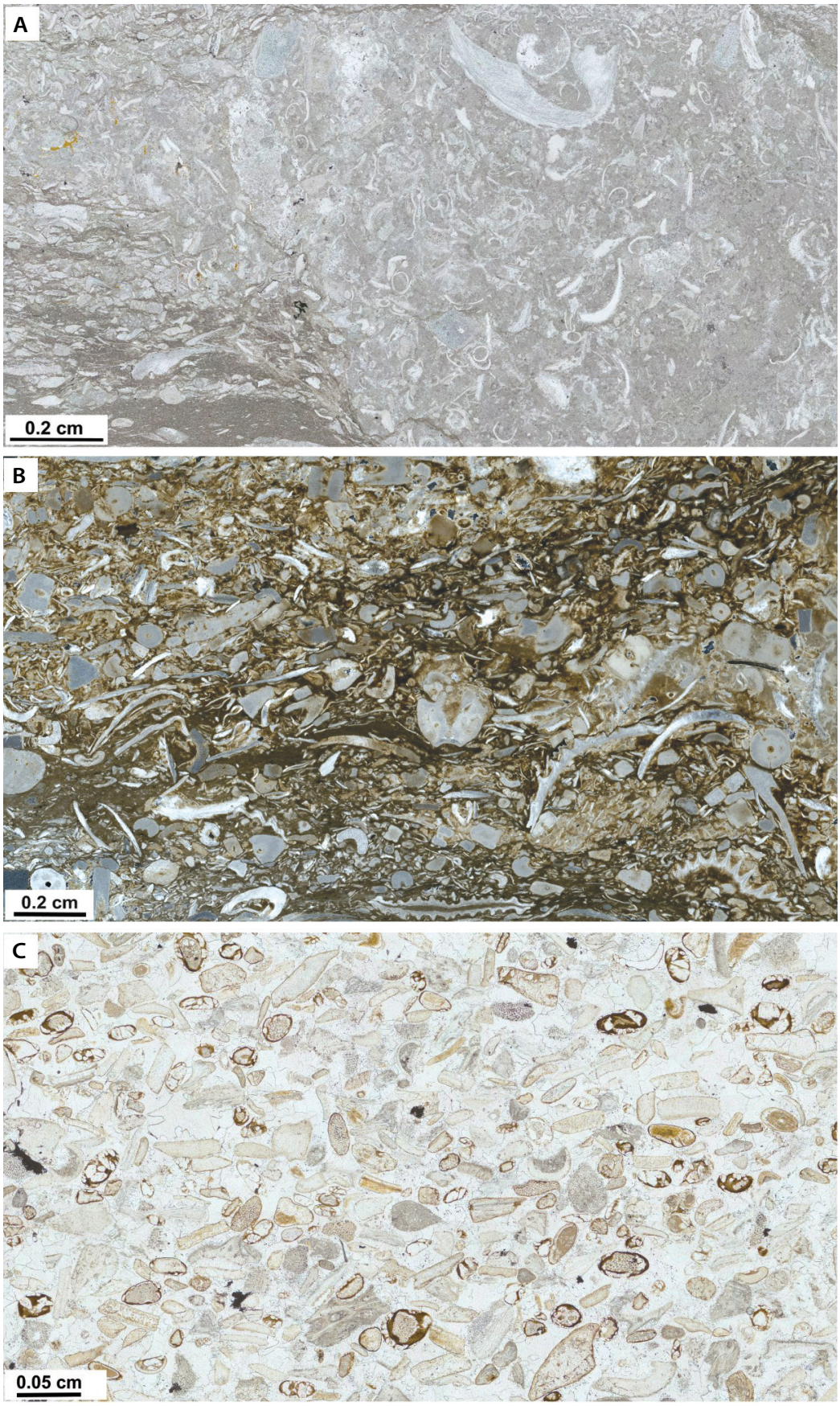
A
0.2 cm
B
0.2 cm
C
0.05 cm

Unit IV and V

Unit IV is composed of oncoid-bearing limestone intercalated with irregular marl beds, where an oncoid floatstone texture prevails (Figs 3, 6). Oncoids vary in size, ranging from less than 1 mm to ~ 2 cm in diameter. Their shapes are diverse, from more regular and symmetrical forms (*e.g.* sub-spherical to elliptical) to highly irregular and asymmetrical types, including incipient oncoids and forms with cloud-like appearances (Fig. 6). Some oncoids show concentric lamination (Fig. 6B). The cortices of oncoids are composed of homogeneous micrite, while the surrounding matrix presents bioclastic-lithoclastic mudstone to wackestone texture (Fig. 6B, C, D, G). Some oncoids exhibit distinct filaments, which could be ascribed to microbial structures of *Rothpletzella* and/or *Girvanella* (Fig. 6C, C1, C2). Clay laminae occasionally accentuate the lamination within the cortex (Fig. 6G). The nucleus is commonly represented by a single bioclast fragment or fossil such as a brachiopod, gastropod, trilobite, bivalve, or coral, although a nucleus may be absent in some cases. Larger oncoids are locally encrusted by a faunal element, such as a bryozoan (Fig. 6C). The matrix commonly contains rhombic dolomite crystals and small mud lithoclasts (Fig. 6B, C, D, G). The bioclastic content of the matrix includes disarticulated and broken shells (primarily brachiopods and trilobites), as well as fragments of bryozoans, corals, echinoderms, and small, often complete ostracods. Other less common components include stromatoporoid fragments, and probable scaphopods, and calcispheres. Although the shape and size of oncoids generally reflect the dimensions of their nuclei, in more densely packed intervals, they also appear deformed by compaction (Fig. 6B, D). Solution seams are common at the contacts between oncoids and bioclasts.

The oncolitic beds are overlain by a few-metre-thick marl interval (Unit V), characterised by a bioclastic mudstone texture, bearing fine-grained limestone nodules/lenses or mottled layers. One such interlayer exhibits a bioclastic peloidal grainstone texture with sparite filling intergranular space (Fig. 6H). The peloids are small and relatively uniform in shape (Fig. 6H), although their origin remains uncertain. Some micritized grains have also been observed. The dominant faunal constituent in this unit is dispersed echinoderm debris, accompanied by disarticulated, rarely complete shells of brachiopods, trilobites, ostracods, and recrystallized molluscs. The marly matrix commonly shows dolomitization and locally contains flakes of organic matter.

Unit VI

The boundary between Unit V and the overlaying Unit VI is abrupt, irregular, and pyritized (Fig. 7C). Unit VI is composed of light grey to grey bioclastic limestones. In the lower part of this complex (~ 5 m), cm to a few dm-bedded bioclastic grainstone (rudstone) is intercalated with subordinate thin dark grey marl beds, which accentuate bedding. The grainstone is interrupted by a ~ 1 m thick marl layer. The dominant bioclasts include echinoderms (mostly crinoids) with abundant brachiopods, accompanied by bryozoans, small ostracod and trilobite shells, corals (rugosa and tabulata), and stromatoporoid fragments. The crinoids occur as individual ossicles and fragments of stems. Grains are poorly to moderately sorted, and broken shells are common. The crinoid syntaxial overgrowths are pervasive (Fig. 7C, D). The interparticle space in rudstone (grainstone) is primarily filled with cement with common small peloids, clay material, or micrite (Fig. 7C, H). Oncoids and marl lithoclasts are also present (Fig. 7C).

From approximately 1060 m depth upwards, the limestone becomes increasingly massive due to the presence of large reef-related bioclasts – stromatoporoid (usually up to 10 cm in size, Fig. 7A, B), crinoid and coral fragments (Fig. 7E–H). The prevailing textures of reefal limestone are floatstone and rudstone (Fig. 7). The occurrence of massive bioclast fragments results in the limestone displaying a rudstone/floatstone texture with a filling matrix comprising bioclastic wackestone/packstone to grainstone (Fig. 7E–H). The faunal contributors in both facies are similar. Solution seams are commonly present at sutured clast contacts, often forming densely layered thin seams parallel to bedding, filled with insoluble residue. A few stylolites were also observed. The fine-grained matrix is often dolomitized. An 8-metre interval overlying the Unit VI was not recovered from the borehole.

Figure 6. Thin sections of the oncoid-bearing facies (unit IV) and overlying marl interval (unit V). • A – macroscopic view (core slab) of oncoid-bearing marl (floatstone texture) with 'cloudy' oncoids (1071.0 m). • B – fitted oncoids within matrix of lithoclastic–skeletal wackestone texture (Viduklė-61, 1147.1 m). Sutured grain contacts resulted in solution seams (irregular brown zones) between oncoids. • C – the elliptical oncoid displaying a longitudinal section of a gastropod (Ga) shell as a nucleus (Viduklė-61, 1143.4 m); C1 – a close-up view of a cyanobacteria (Cy) displaying a well-developed tubular structure (*Rothpletzella*) and organoclast filled with calcite cement (Or); C2 – fenestrate bryozoan (Br) and filamentous cyanobacteria (Cy) encrusting oncoid. • D – oncoids exhibiting different size ratios of nucleus and cortex thicknesses or lack of a core (1073.1 m). Compaction is expressed in the form of suture seams between grains. E – coral fragment as the nucleus of oncoid (1071.2 m). F – well preserved brachiopod shell showing the internal spiralia (1076.0). • G – echinoderm debris incorporated into the oncoid cortex possibly during transport (1074.2 m). • H – close up view of limestone interlayer within marly unit V representing peloidal grainstone with bioclasts *i.e.* fragment of crinoidal stem, brachiopod (top) and partly recrystallized gastropod (bottom) shells (1067.0 m). • I – geopetal structure in peloidal grainstone evidencing deposition of crinoid particles on brachiopod shell.

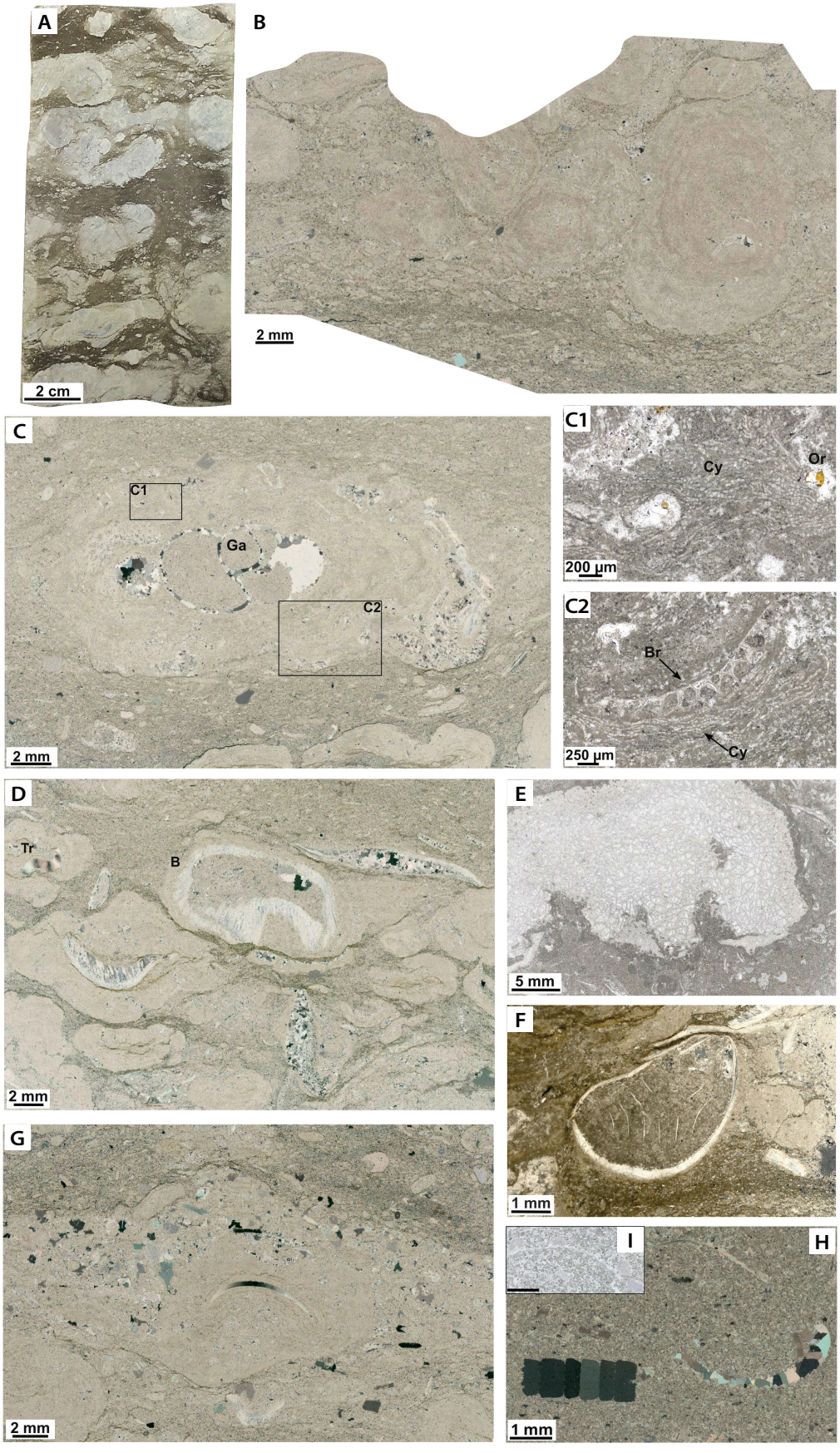
A
2 cm
B
2 mm
C
C1
Ga
C2
2 mm
C1
Cy
Or
200 µm
C2
Br
Cy
250 µm
D
Tr
B
2 mm
E
5 mm
F
1 mm
G
2 mm
I
H
1 mm

Unit VII

Unit VII represents the upper portion of a potentially thicker lithological unit that was not fully recovered from the borehole (Fig. 3). It is characterized by a fine lamination to cm-scale interbedding of light grey limestone and greenish marl (Fig. 8). The prevailing facies exhibit a dolomitized mudstone texture, locally enriched with abundant intraclasts. The laminae are often discontinuous, ranging from planar and sub-planar to wavy and irregular, sometimes resembling lenticular-like and cross-lamination morphologies (Fig. 8B1). Bioclastic content is low, and of limited diversity, comprising predominantly often broken, reworked, and bored shell fragments – usually ostracods, with minor admixture of other skeletal particles.

In the upper few decimetres of Unit VII, these laminated facies shift to massive light grey lime mudstone/wackestone (Fig. 9E, F), containing poorly sorted shell fragments of typically ostracods and molluscs. Articulated small ostracods are common, often displaying sparry cement infill or geopetal structures (Fig. 9F). Crinoids, frequently surrounded by syntaxial overgrowths, are present, but frequently occur in association with lithoclasts (left upper corner in Fig. 9F). The limestone also contains irregular sparite-filled voids, suggestive of fenestral (birdseye) fabrics (Fig. 9F). However, some more regular shapes resemble shell moulds filled with coarse sparite and could represent leached skeletal fragments. Some skeletal grains show only ghost textures due to fine recrystallization. Irregular dark patches/bands within the mudstone and random orientation of bioclasts are attributed to bioturbation (Fig. 9E, F).

In the uppermost few centimetres, the limestone is deformed and brecciated, showing intense sub-horizontal cracks partly filled with a mixture of clay, quartz, dolomite, feldspathic grains, and organic matter (Fig. 9C, D). An unidentified dark reddish material, likely representing iron-rich precipitation, occurs along the cracks. Microfacial examination revealed mudstone-wackestone texture with predominantly crinoids and crinoid detritus, with scattered large ostracod fragments (Fig. 9D). Crinoid debris shows syntaxial overgrowths (Fig. 9D). The mudstone contains elongated, bedding-parallel fenestral voids, connected to sub-vertical spar-filled fractures. The upper boundary of this mudstone is penetrated by cracks filled with sedimentary material from the overlying layer, indicating synsedimentary fracturing (Fig. 9B). The cracked limestone interval is overlain by a few cm thick interval of irregularly interbedded dolomitized greenish marl and grey limestone, showing mudstone-wackestone texture (Fig. 9A, B). This interval is faunally low in diversity, and contains abundant disarticulated and fragmented ostracod shells, along with echinoderm debris, single corals, and intraclasts (Fig. 9B). Shells are often sub-parallel to bedding, locally forming cap-in-cap structures (Fig. 9B). Some ostracod shells exhibit sheltered spar-filled cavities, interpreted as cement growth in vacant microenvironments (Fig. 9B). Disrupted beds point to a certain degree of bioturbation (Fig. 9A). The transition to the overlying Unit VIII (Ventspils Fm.) is abrupt, marked by a clear lithological change to nodular/lumpy limestone (Fig. 9A, in the upper part), suggesting a possible erosional boundary.

Unit VIII

Unit VIII is, in general, represented by light to medium grey limestones. In the first ~ 4 m of the section, slightly nodular to a few cm-bedded undulating fabrics are observed (Fig. 9A, upper part of the hand specimen), and they are interlayered/surrounded by frequent thin dark brownish grey marl beds. Here, local shell enrichment is observed. Up section, the limestone grades into more massive dm-bedded fabric, with bedding-parallel and wavy parting of dark brownish grey to black marl beds up to a few centimetres in thickness. This unit is interrupted by a ~ 2 m-thick facies of generally laminated/thin-bedded grey limestone and greenish grey marl (Fig. 10F, G; at ~ 1031–1033 m depth). In the unit, the dark colour of marls reflects a high content in organic matter, and bioclastic material is commonly accumulated within them. The limestones are partly dolomitized and unevenly clayey. Fractures and vugs are present.

Several microfacies were distinguished in this unit. A nodular/wavy bedded limestone interval is represented by bioclastic wackstone. The limestone and marls appear to contain a similar fossil assemblage characterised by

Figure 7. Bioclastic limestone. • A – reefal limestone mainly composed of large stromatoporoids, corals and echinoderms (1058.2 m). • B – large porous clast of stromatoporoid (1060.7 m). • C – boundary between bioclastic limestone (unit VI) and underlying unit V showing the bottom of non-reefal bioclastic limestone: bioclastic–peloidal grainstone–rudstone (1065.5 m). Intensive pyritization of bioclasts (black colour). • D – large rugose coral within crinoidal–bioclastic grainstone. Solution seams between the grains (1065.2 m). The grainstone is almost fully cemented with syntaxial calcite. • E – bioclastic floatstone with bryozoan dislocated by fracture (arrow) within bioclastic wackestone matrix (1056.0 m). • F – stromatoporoid floatstone with crinoid and brachiopod–rich wackestone–packstone matrix (1059.0 m); an argillaceous micritic matrix shows patchy, locally strong dolomitization. • G – stromatoporoid rudstone with crinoidal grainstone–packstone matrix (1052.1 m). • H – stromatoporoid–coral rudstone (1058.0 m). Fossils are fitted and mostly represented by massive stromatoporoid fragments and corals (rugosa and tabulate) with numerous crinoid ossicles, occasional brachiopod and trilobite particles. The pore space between the clasts is partly filled with clay. Sutured grain contacts between the clasts. The limestone shows some degree of brecciation.

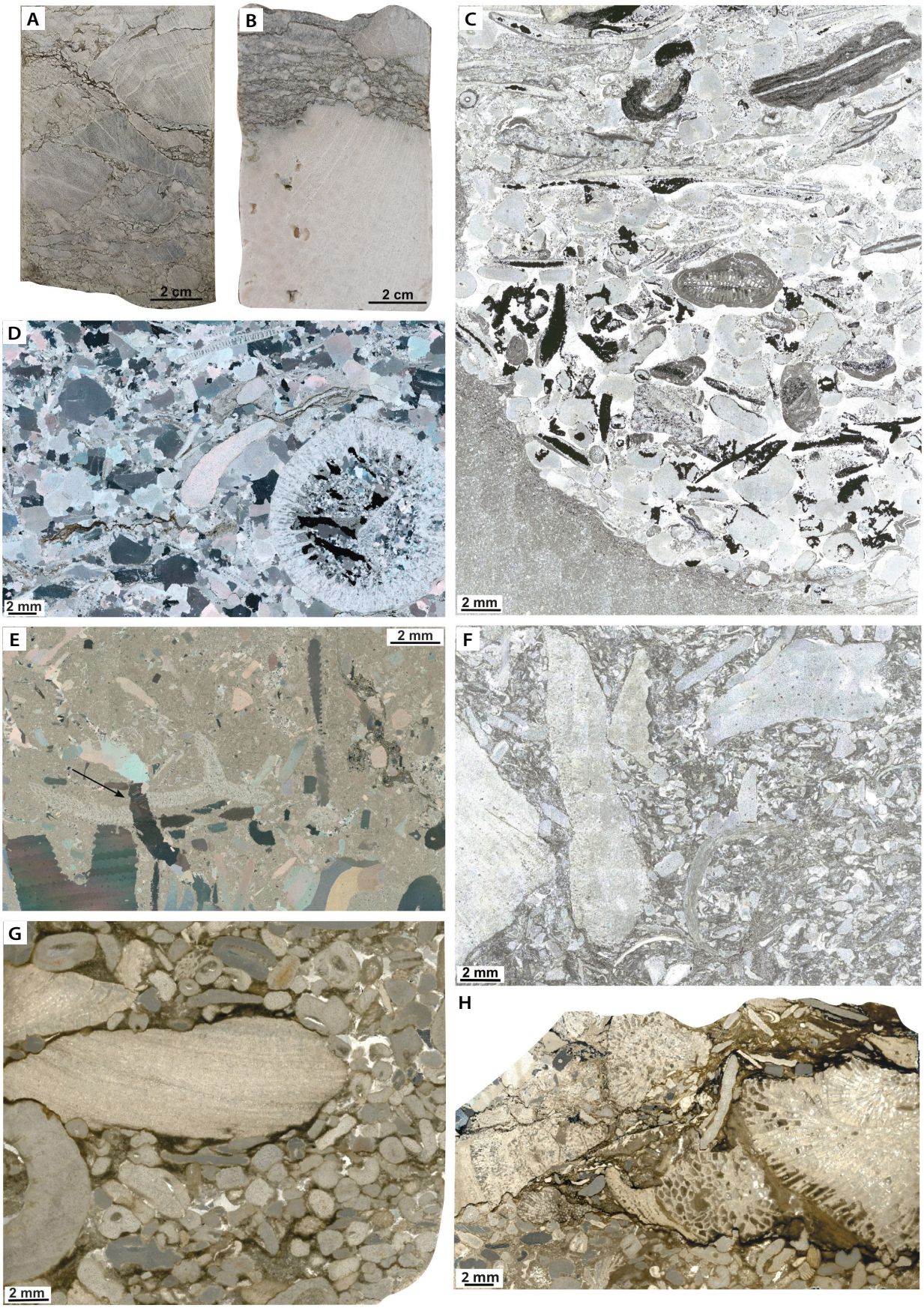
A
2 cm
B
2 cm
C
2 mm
D
2 mm
E
2 mm
F
2 mm
G
2 mm
H
2 mm

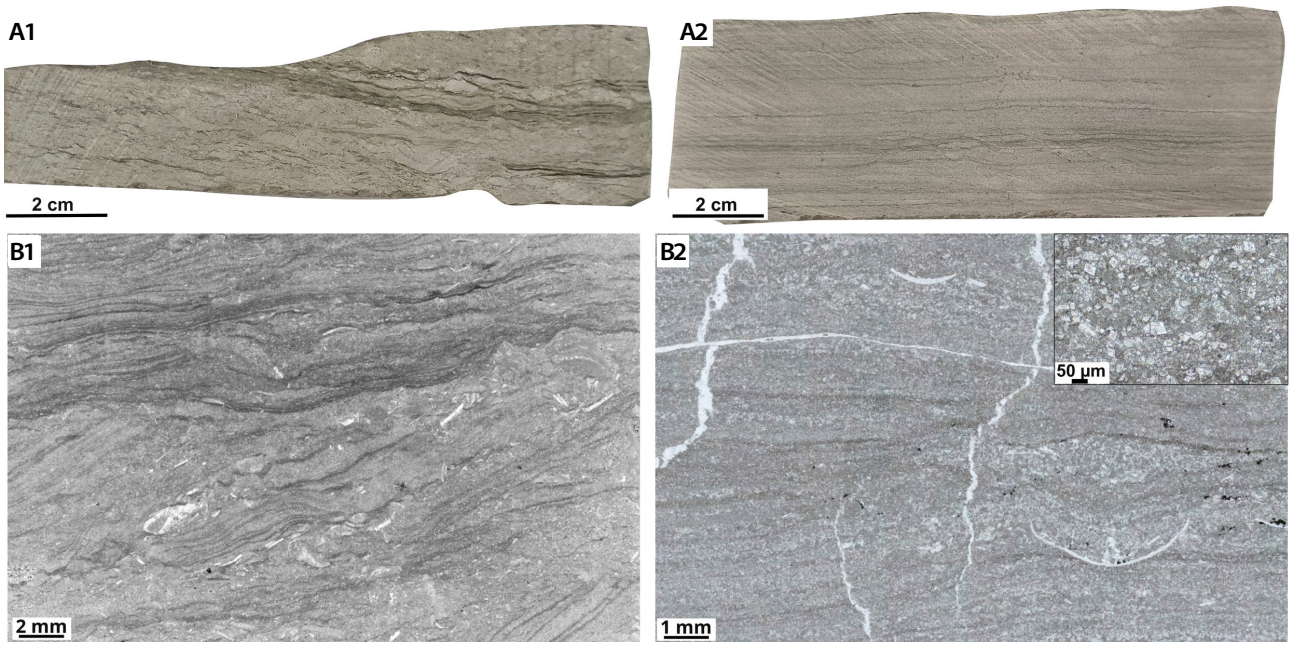

Figure 8. Marl–limestone alternation of the unit VII. • A1, A2 – hand specimen (1043.6, 1042.9 m), • B, B1 – thin section showing truncated surface, laminated intraclast and minor scattered fragmented shells and intraclasts (1043.6 m); B2 – slightly undulating planar lamination of facies with occasional ostracod fossils (1042.9 m). Rock displays ubiquitous dolomitization (close-up view in B2).

mostly poorly sorted diverse shell components – disarticulated and fragmented detritus of brachiopods, ostracods, trilobites, as well as echinoderms, gastropods, fragments of stromatoporoid, with minor larger bioclasts including well preserved disarticulated large ostracods or brachiopods. Marl interbeds often contain a tight accumulation of thick-walled brachiopod shell fragments (Fig. 10D, partly enhanced by compaction). Beds of bioclastic-peloidal grainstone/rudstone are present as well (Fig. 10A, A1, A2). Grainstone is marked by distinct and pervasive peloids and grain micritization. Some of the peloids probably originated from micritized bioclasts, although faecal pellets are also thought to contribute to the overall peloidal fabric. The faunal assemblage includes coarser components, typically including bivalves, gastropods, ostracods, and brachiopods, while the finer fossils are represented by small ostracods, echinoderms. Molluscs are recrystallized. Up section, bioclastic wackestone shows better preserved shell fragments, indicating much less intense reworking with common ostracods, gastropods, bivalves, brachiopods, crinoids, less frequent trilobites, and single fragments of bryozoan or coral. Molluscs are recrystallized, while some shells show borings, micritic rims, or complete micritization. The rock may also show bimodal bioclastic distribution with the largest grains involving gastropods, bivalves, and ostracods, thus demonstrating a floatstone texture. In specific intervals, coarse coral fragments and oncoids (up to ~ 2 cm in diameter) are accumulated (Figs 3; 10E). Oncoids may lack a core or contain bioclasts as nuclei, such as gastropod or bivalve (Fig. 10E). Although traces of microbial structures are observed within the oncoids, partial recrystallization of the oncoids does not allow for further identification. Oncoids display shapes from subspherical to elongated forms, generally determined by the shape of the nucleus (Fig. 10E). Clumps and filaments

Figure 9. Facies variability across the boundary of the Mituva and Ventspils Fm. evidencing subaerial exposure. • A, C, E – hand specimen showing the uppermost interval of the unit VII arranged according to depth. The bottom of the interval starts with lime mudstone with inferred fenestrae fabrics (E – 1041.7 m). Corresponding close-up view of thin section (F) illustrating irregular few mm-sized sparite-filled voids in mudstone, which are interpreted as birdseyes. In the left upper corner in Fig. 9F – intraclast containing crinoids with common syntaxial overgrowths. C – cracked limestone (1041.6 m), and corresponding thin section (D) of lime mudstone–wackestone with crinoids, densely covered with sub-horizontal cracks. Reddish–browish material along the cracks probably refers to iron precipitations. • B – thin section of bioclastic lime mudstone–wackestone irregularly interlayered with greenish marl (1041.5 m). Dominant fauna are large ostracods and crinoids. The lower part of this picture shows the underlying cracked mudstone that is cut by a crack filled with sediments from the overlying bed. Note the coral fragment at a funnel-shaped inlet to the crack (arrow). Some layers are disrupted or mottled, probably due to bioturbation (see lower half of Fig. A). A sharp lithology changes to nodular/lumpy limestone of unit VIII (Ventspils Fm.) can be seen in A.

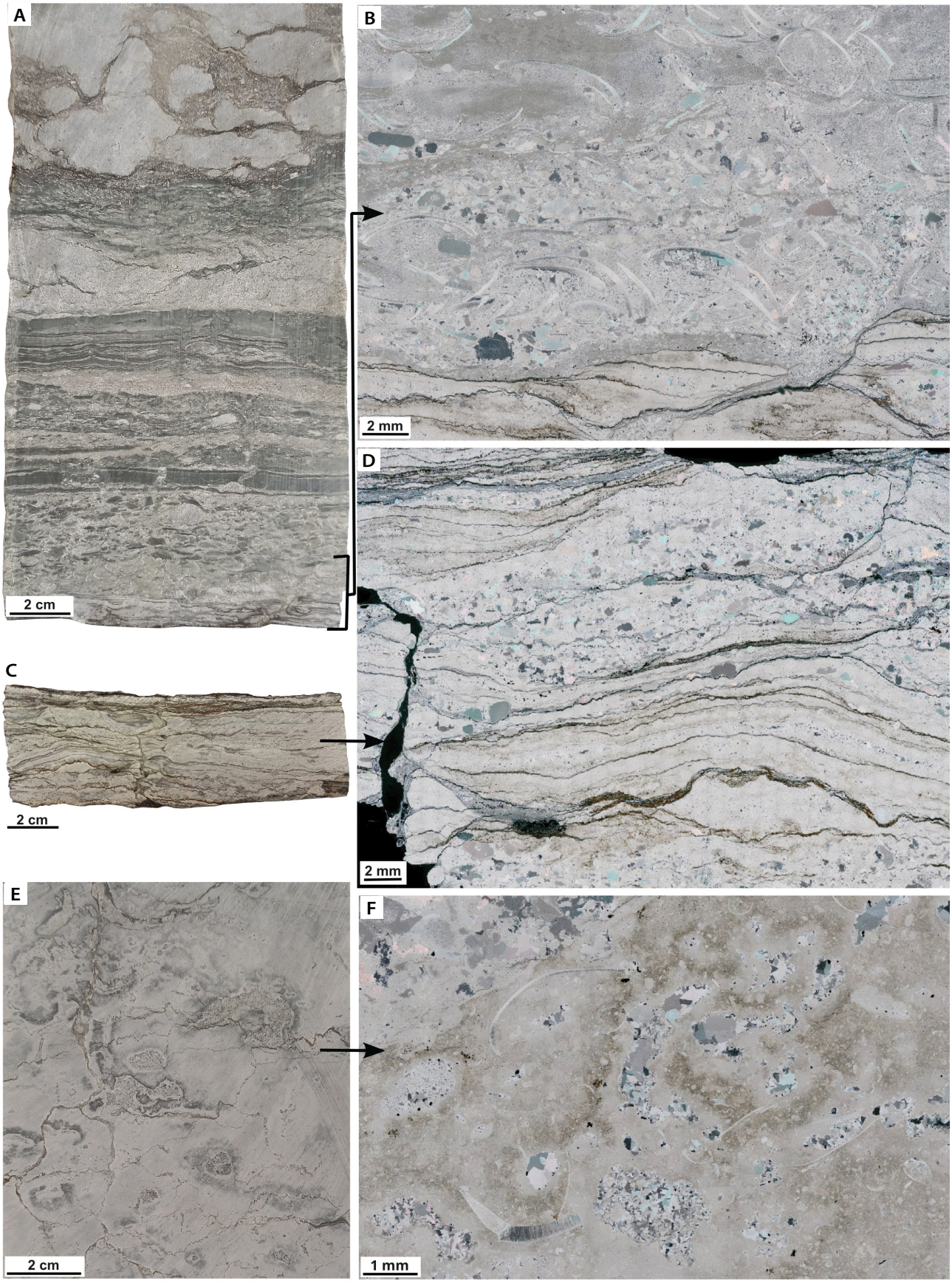
A
2 cm
B
2 mm
C
2 cm
D
2 mm
E
2 cm
F
1 mm

of amorphous organic matter are common within the section (Fig. 10A, E). Matrix recrystallization to micro or pseudospar is a common occurrence within the unit, and often obliterates textural and compositional features. The peloidal-like texture appears frequently within recrystallized areas and is thought to be related to mould peloids and remnants of unaltered micrite.

A ~ 2 m-thick facies of limestone-marl laminated to thin-bedded alternation is classified as lime mudstone to wackestone with irregularly distributed echinoderms (commonly crinoids) and their detritus, accompanied by intraclasts, sparse fragmented shells, and single bryozoan or coral fragments (Fig. 10F, G). The rock is partly dolomitized, and syntaxial overgrowths around crinoids are common. The laminae are frequently discontinuous or disrupted, lamination planar to wavy, with present cross-lamination (Fig. 10F, G). This facies association also includes bioclastic wackestone with micritic matrix showing signs of recrystallization, and irregular argillaceous laminae. It contains echinoderm, mollusc, brachiopod, and ostracod components of varying sizes.

Within the overlying interval, a bioclastic mudstone to wackestone was identified with dominant presence of gastropod, bivalve, ostracod, and crinoid components (Fig. 10B). The rock has been affected by recrystallization. Brownish clumps and unidentified particles, likely referring to organic matter, were observed. Large, massive fragments of stromatoporoids, accompanied by brachiopods and some corals and bryozoans, are encountered especially in the uppermost few metres of the unit, where stylolitisation is well expressed, commonly between the stromatoporoid fragments.

Conodont biostratigraphy

The conodont material revealed a number of stratigraphically restricted taxa (Appendix 1, Fig.11), whose distributions closely approximate those in other sections of the Silurian Baltic Basin. Recurrence plots (Figs 12, 13) and cross-recurrence plots (Fig. 14) were used for stratigraphic correlation. Zonal species such as *Kockelella variabilis*, *Ozarkodina baccata*, *Jeppssonia crispa* (*Jeppssonia* is a recently rectified genus combining *snajdri–parasnajdri–crispa* species complex, Barrick *et al*. 2024), and a "disaster taxon" *Panderodus equicostatus* are of the highest importance in the estimation of correlation lines. The regionally persistent patterns of community compositions also provide additional information on the exact paths of correlation lines, which were estimated using the DTW algorithm on cross-recurrence matrices. Based on the experiments on the estimation of correlation lines using different recurrence rates, it can be seen that depending on the position in the section there can be up to several metre differences in correlation paths (Fig. 13). The greatest uncertainty is encountered in determining the exact thickness of the *Polygnathoides siluricus* Zone (Fig. 14), the position of which is estimated based on the distribution of other taxa, as this species was not recorded in the Lapgiriai-1 core.

One of the best stratigraphically constrained parts of the core corresponds to the *P. latialata–Jeppssonia snajdri* Interval Biozone, where in all three cores – Viduklė-61, the Lapgiriai-1, and Milaičiai-103 (Spiridonov *et al.* 2017b) – a compositionally "time anomalous" episode, characterised by a low species richness assemblage is dominated by *Panderodus equicostatus* – distinct black squares almost non-recurring with other time intervals in both recurrence (Figs 12, 13) as well as in cross-recurrence plots (Fig. 14). The uppermost part of the section is typified by the co-occurrence of *Jeppssonia crispa* and *Ozarkodina baccata*, which, together with *Ctenognathodus* sp. and robust *Ozarkodina svetlanae* form a typical shallow-water assemblage of the uppermost Ludfordian in the eastern part of the Silurian Baltic Basin – distinguished as the *baccata–crispa* Zone (Spiridonov *et al*. 2017b, 2020a). Here, the uppermost part of the section can also be correlated with a rather high degree of precision in relative terms (Fig. 15).

The abundance trends in Viduklė-61 and Lapgiriai-1 core sections show superficial similarities with low abundance in the beginning and higher average abundances in the upper part of the *variabilis* Zone (Fig. 16), while having drops in abundance in the *siluricus* Zone and again high abundance in the upper part of the *siluricus* Zone. Both sections in the upper part of the Ludfordian are characterised by low conodont abundances. Although conodont abundances in both sections show heavy-tailed power law-like histograms, one cardinal difference between the abundance structures in those sections lies in the

Figure 10. Facies of the Ventspils Fm (unit VIII). • A – bioclastic–peloidal grainstone and common shells with micritic rims (1039.3 m); A1 – close-up view of a fenestrate bryozoan fragment within peloidal matrix; A2 – gastropod shell with partial pyritization (black colour). • B – bioclastic wackestone with numerous shells of bivalves (arrow), gastropods, ostracods and their fragments, as well as crinoids (1028.0 m). • C – small stromatoporoid penetrated with bands of sediment, which probably includes fragments of coral (arrow, 1041.1 m). • D – marl interbed rich in fragmented shells of large brachiopods, single coral and graptolite (black, 1039.8 m). • E – reworked coral (C) fragments and oncoids (On) within marly matrix (1035.7 m). Such accumulation of coarse clasts could be storm–induced. • F – a core hand-specimen displaying limestone–marl fine alternation with evident disruption of lamina, likely attributable to the process of slumping of semi–lithified material (1031.7 m). • G – thin section of the corresponding laminated interval (F) with echinoderms showing cross-lamination.

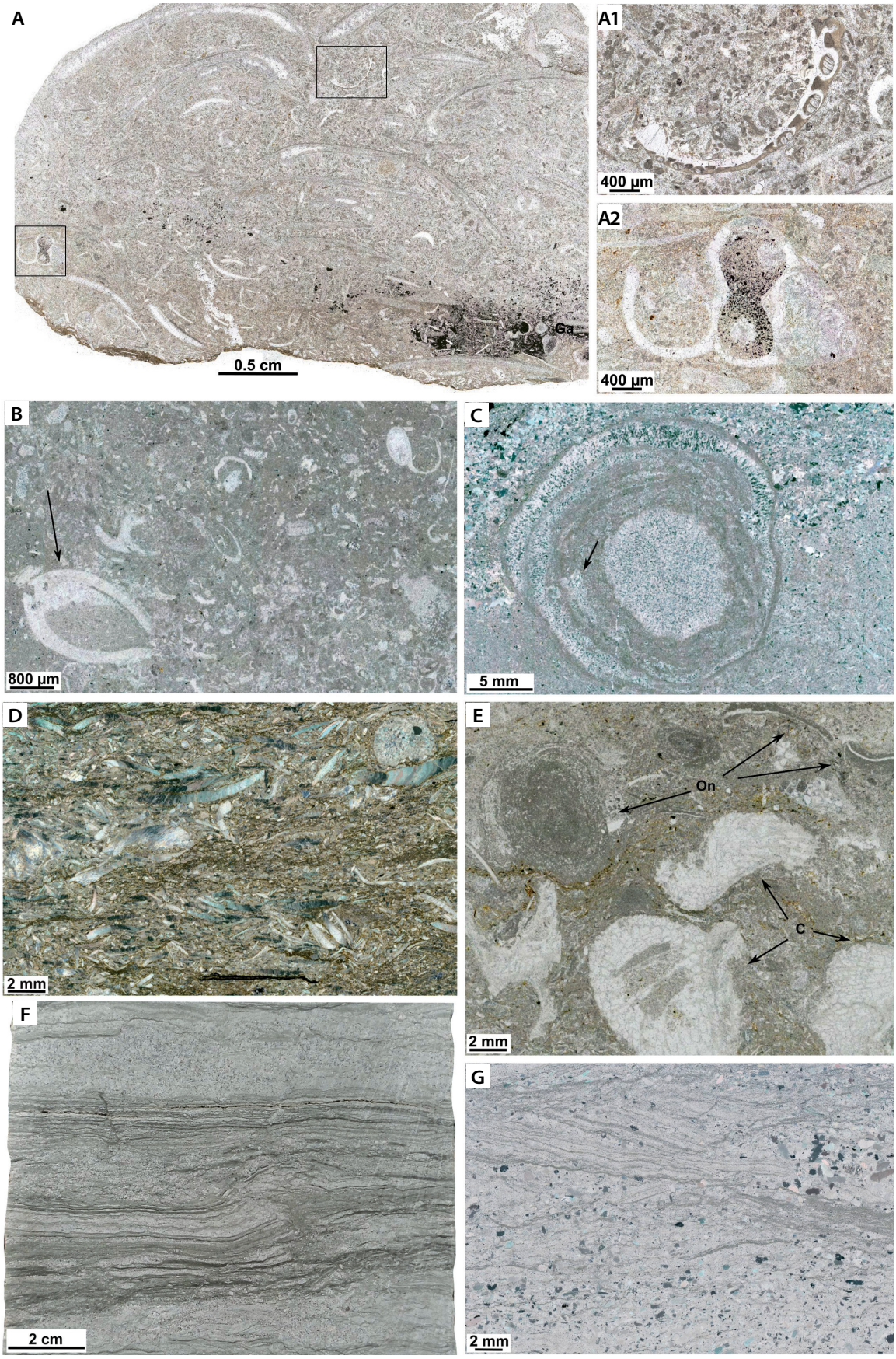
A
Ga
0.5 cm
A1
400 µm
A2
400 µm
B
800 µm
C
5 mm
D
2 mm
E
On
C
2 mm
F
2 cm
G
2 mm

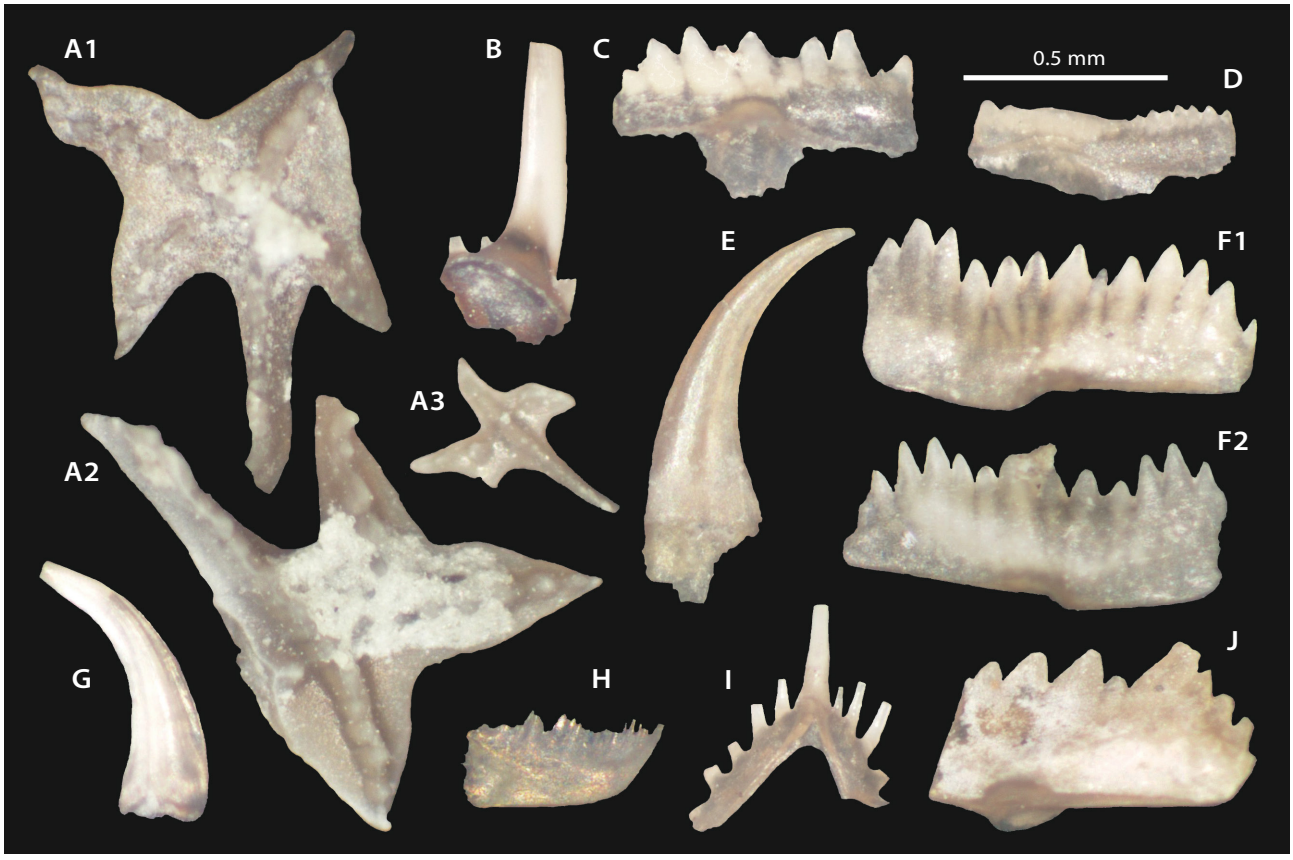

Figure 11. Ludlowian conodonts from the Lapgiriai-1 core. • A – *Kockelella variabilis* Walliser, 1964, oral view of specimens; A1 – VU–CON–LAP1–001; A2 – VU–CON–LAP1–002; A3 – VU–CON–LAP1–003; depth 1118 m. • B – *Coryssognathus dubius* (Rhodes, 1953), Pb element No. A3 VU–CON–LAP1–004, depth 1100 m. • C – *Ozarkodina baccata* Miller & Aldridge, 1997, Pa element No. A3 VU–CON–LAP1–005, depth 1039 m. • D – *Jeppssonia crispa* (Walliser, 1964), Pa element, No. A3 VU–CON–LAP1–006, depth 1035.3 m. • E – *Panderodus equicostatus* (Rhodes, 1953), No. A3 VU–CON–LAP1–007,depth 1081 m. • F – *Ozarkodina confluens* Branson & Mehl, 1933, Pa elements; F1 – No. A3 VU–CON–LAP1–008, depth 1035.3 m; F2 – No. A3 VU–CON–LAP1–009, depth 1039 m. • G – *Panderodus unicostatus* (Branson & Mehl, 1933), No. A3 VU–CON–LAP1–010, depth 1100 m. • H – *Belodella resima* (Philip, 1965), No. A3 VU–CON–LAP1–011, dept1 1100 m. • I – *Oulodus elegans* (Walliser, 1964), Sa element, No. A3 VU–CON–LAP1–012, depth 1026 m;. • J – *Ctenognathodus murchisoni* (Pander, 1856), Pa element No. VU–CON–LAP1–012, depth 1027 m.

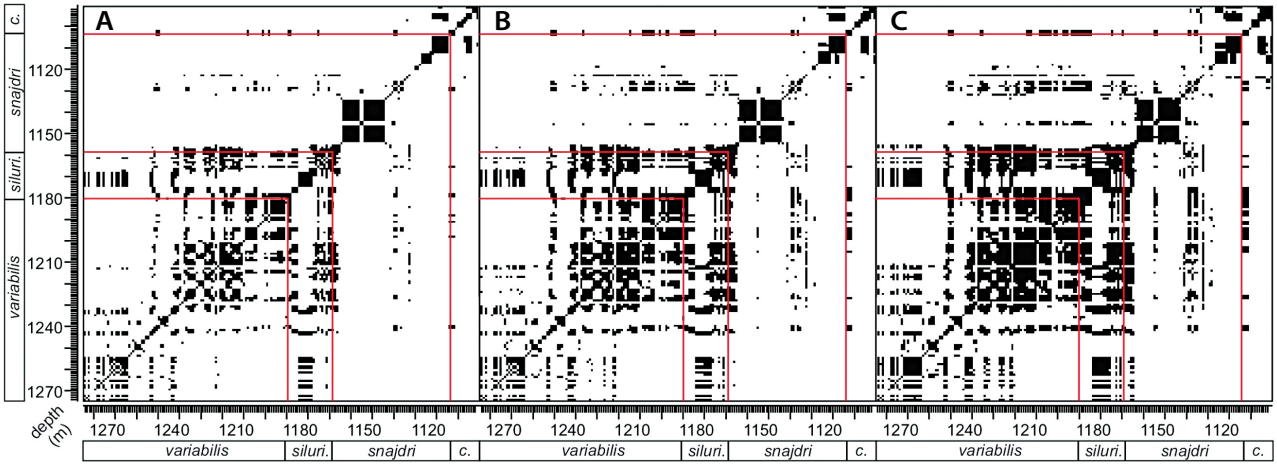

Figure 12. Autorecurrence plot of Viduklė-61 conodonts based on the Morisita–Horn similarity of assemblages with different recurrence rates (similar states shown in black); A – 10%; B – 15%; C – 20%. Black squares around the diagonal line show the increased self-similarity of samples in a given time interval. The sizes and locations of these squares show the durations and the distribution of these self-similar states, as well as sharp changes between them, which can either indicate the change in sampling and biotic turnover events.

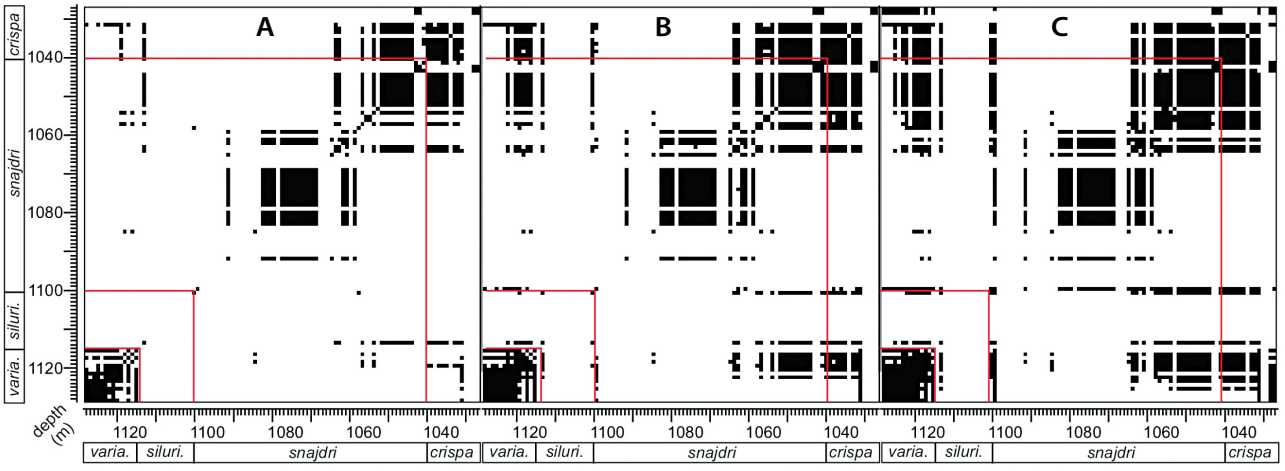

Figure 13. Autorecurrence plot of Lapgiriai-1 conodonts based on the Morisita–Horn similarity of assemblages (similar states shown in black) with different recurrence rates (RR) at A – 10%; B – 15%; C – 20%. Lower values of RR filter for increasingly more similar combinations of stratigraphically organized samples in a "time series", and conversely if we use higher values of RR in the construction of the recurrence plot the value of similarity is defined more liberally (later definition could be useful in the case where there is high degree of the measurement/sampling noise, which is frequent situation in the real stratigraphical sample series).

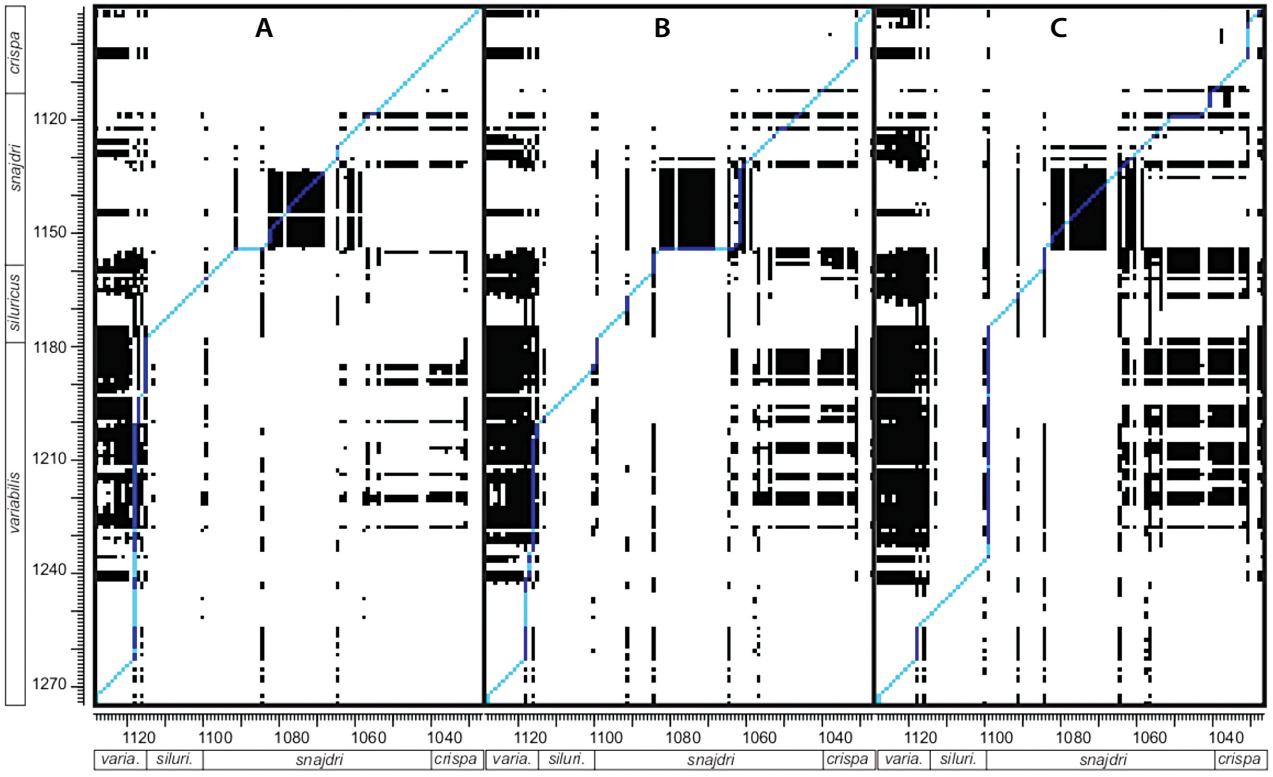

Figure 14. Cross-recurrence plots with DTW (Dynamic Time Warping) derived lines of correlation between Viduklė-61 and Lapgiriai-1 cores using different recurrence rates at A – 10%; B – 15%; C – 20%. Lines show the optimal paths of correlation through the cross-recurrence (and more generally cross-similarity between cores) matrices.

number of barren samples. Samples with "0" abundance compose only a minor fraction of Viduklė-61 samples (6.6%), while in the Lapgiriai-1 section, barren samples were nearly as frequent as productive samples (42%). It should be noted that lacunae in conodont distributions are clustered, particularly in strata corresponding (according to the stable carbon isotopic curve) to the Lau Event. Therefore, this factor alone would limit the accuracy of the inferred correlation lines, regardless of the estimation method used.

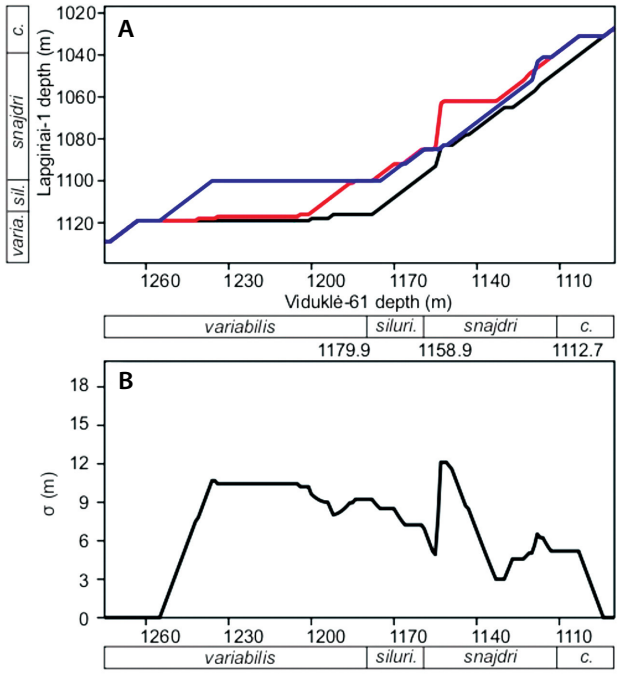

Figure 15. A – stratigraphic variations in the line of correlation as a function of recurrence rate in cross-recurrence plots between Viduklė-61 and Lapgiriai-1 sections. • B – change in standard deviation between correlation lines in the Lapgiriai-1 section as a function of the position in the Viduklė-61 section.

Graptolite distribution

The graptolites are rare within the examined interval of the Lapgiriai-1 borehole. The collected graptolites are concentrated in a marl layer in the uppermost part of the Dubysa Formation (1101.5–1105.9 m interval; Fig. 3). Only *Pristiograptus dubius frequens* Jaekel subspecies was found there. The distinguishing characteristic of this subspecies is the presence of four or more rings of the sicula (Fig. 18), as noted by Urbanek *et al.* (2012). This feature allows for the differentiation of this subspecies from other members of the *dubius* group, specifically the pristiograptids. *Pristiograptus d. frequens*, which has a long-stratigraphic range, extending from the uppermost Homerian *nassa* Biozone to the middle of Ludfordian *tenuis* Biozone, and it persists until the Lau Event as the last graptolite representative of the dubius group (Radzevičius *et al*. 2023).

$\delta^{13}C$ stratigraphy

The carbon isotope composition of carbonate for the collected samples varies between −0.32 and +7.51‰ (Fig. 3). The isotope record begins with a series of relatively stable values around the baseline of 0‰ along Units I and II (Dubysa Fm.), which correspond to *K. variabilis* and inferred *P. siluricus* conodont zones. A minor increase, reaching up to ~ 3.3‰, occurs near the boundary between these two zones. From the uppermost part of Unit II, which coincides with a 2-metre-thick limestone bed, the curve of $\delta^{13}C_{carb}$ over the next ~ 20 metres reaches the most positive values – between 6.63‰ and 7.51‰, in the interval that corresponds to the oncolitic beds (Unit IV within the Mituva Fm.) of the *P. latialata–Jeppssonia snajdri* Interval Biozone. Up section, the $\delta^{13}C$ values gradually decline, returning to baseline levels in the lower part of Unit VIII (Ventspils Fm.), which corresponds to *Oz. baccata–J. crispa* Zones. This is followed by a minor positive excursion of $\delta^{13}C_{carb}$ with values rising by 1.2–1.4‰ in the upper part of Unit VIII. Oxygen isotope values

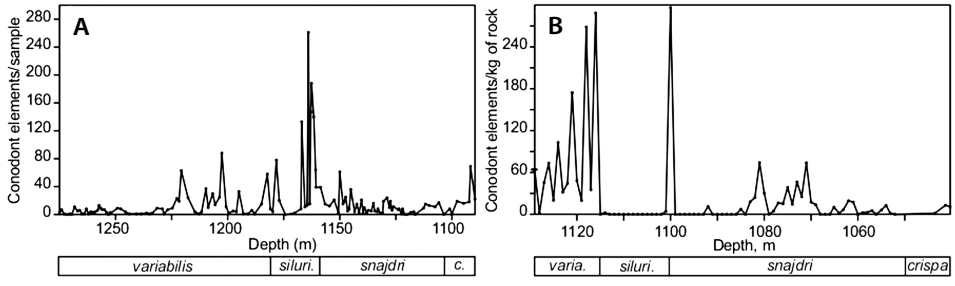

Figure 16. Changes in abundance of conodont elements as a function of depth. • A – Viduklė-61 (conodont elements per sample). • B – Lapgiriai-1 (conodonts per kg of rock).

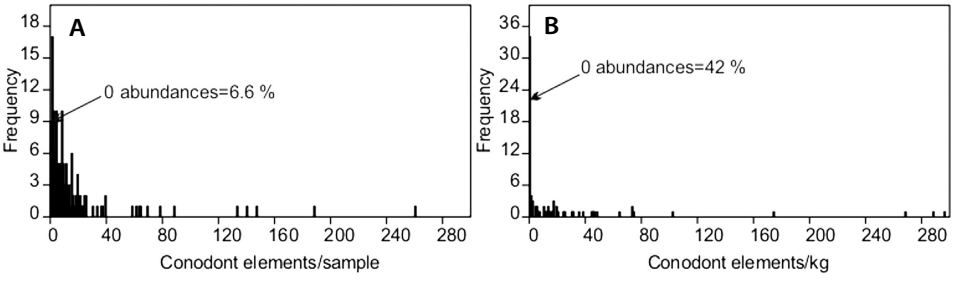

Figure 17. Histograms of conodont abundance. • A – Viduklė-61 (conodont elements per sample). • B – Lapgiriai-1 (conodonts per kg of rock). All histograms scaled that each bin category was rounded to the integer value. The first column in the histogram shows the number of samples with "0" abundance, or in other words barren with respect to conodont elements samples.

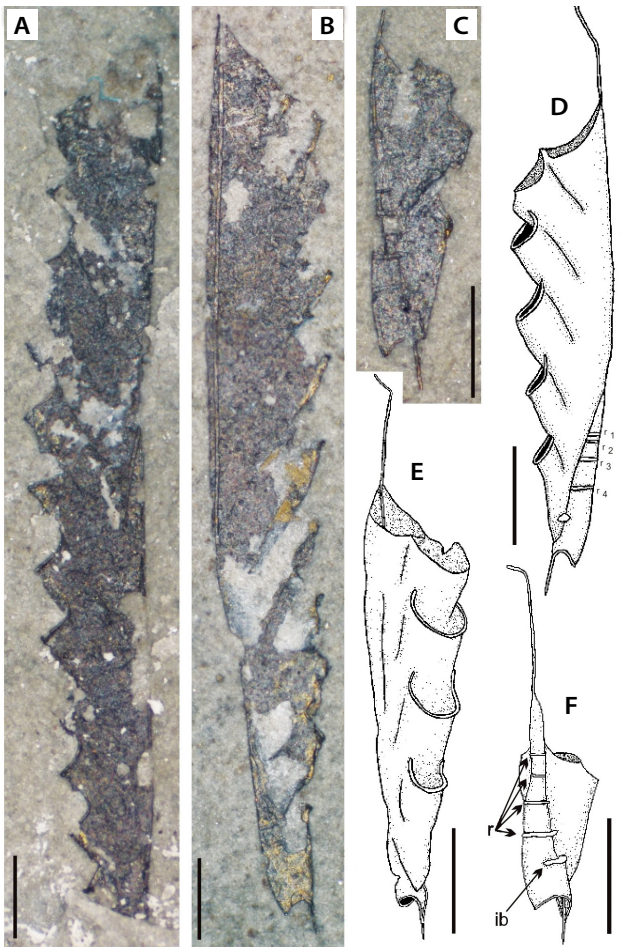

Figure 18. *Pristiograptus dubius frequens* Jaekel from Ludfordian, Dubysa Regional Satge, Dubysa Formation, Nova Beds of Lapgiriai-1 borehole Lithuania. A – no. VU–LAP–1–04, depth 1101,9 m. B – no. VU–LAP–1–05, depth 1103.4 m. C – no. VU–LAP–1–02, depth 1104.9 m. D–F isolated rhabdosomes; D – no. VU–S.L–1–436, depth 1101.9 m; E – no. VU–S.L–1–437, depth 1101.9 m; F – no. VU–S.L–1–438, depth 1104.9 m. Scale bar = 1 mm. Abbreviations: ib – initial bud; r – rings of sicula.

($\delta^{18}O_{carb}$) were also recorded, but were not analysed within the scope of this study (Fig. 3, Appendix 2).

Sediments and rocks are subject to post-depositional processes that may alter their primary geochemical signatures. However, a low degree of thermal alteration (CAI 1) rules out thermal overprinting as a major influencing factor in this case. A cross-plot of the entire dataset (n = 95) of $\delta^{13}C_{carb}$ versus $\delta^{18}O_{carb}$ indicates no correlation ($R < 0.1$, Appendix 2), nevertheless, a closer examination of the data revealed moderately strong covariation within specific intervals, with $R = 0.68$ ($p < 0.05$) for an interval 1080–1100 m and $R = 0.56$ ($p < 0.05$) for an interval 1052–1079 m (Appendices 2, 3). These patterns may reflect some amount of diagenetic changes in the isotopic record, potentially due to processes such as dolomitization or recrystallization.

Discussion

Depositional settings

The identified sedimentary facies and their vertical succession along the borehole profile suggest that a carbonate ramp system dominated the study area during the Ludlow. The fine-grained facies belonging to units I, II, and III indicate hemipelagic sedimentation under relatively quiet-water conditions. The sediments were deposited below the storm wave base; therefore, it is placed in an outer to lower mid ramp location. Sedimentation in distal ramp settings is characteristic of the deposition of marl-limestone alternation, and microfacies of skeletal packstone to wackestone textures (*e.g.* Burchette & Wright 1992, Machel & Hunter 1994, Flügel 2010). In general, the facies show rather uniform development. Nevertheless, they also manifest differences in content and grain size of bioclastic components, which is indicative of a proximity to the carbonate platform, the presence of event beds, or evidence of condensed intervals. Part of the skeletal material was probably derived from the shallow ramp zone during high-energy events, while part of the bioclasts was autochthonous. Fine-grained carbonate beds/nodules are common in these facies. Whether bipartite lithologies (limestone nodules/beds embedded within marl matrix) represent a direct response to changes in environmental conditions remains a subject of debate. The nature of such sedimentation could be explained by the differential diagenesis model (Westphal 2006), which involves the dissolution of aragonite particles in marl layers and subsequent calcite cementation in limestone layers taking place during marine burial diagenesis. While a more comprehensive study is required to determine the genesis of these bipartite lithologies in the studied section, observations of the folding laminations in the mudrock surrounding the nodules suggest that at least part of them most likely formed during early diagenesis prior to deeper burial and physical compaction.

Thin beds of a bioclastic packstone-grainstone are present in a limestone interval, which is embedded within a thick marl complex of a distal ramp (Fig. 5). Their microfacies characteristics allow them to be ascribed to RMF 26 and 27 microfacies types of a carbonate ramp (Flügel 2010), referring to high-energy carbonates and shoals. These sediments originated in mid- to inner-ramp locations, but their occurrence within marly facies is possibly storm-induced or the result of washed-out accumulation.

Mud-supported textures of oncoid-rich limestone-marl alternations of Unit IV and marls comprising Unit V indicate deposition occurring in a relatively quiet-water regime below the fair-water wave base within mid-ramp settings. The embedding of oncoids in a matrix that is clearly

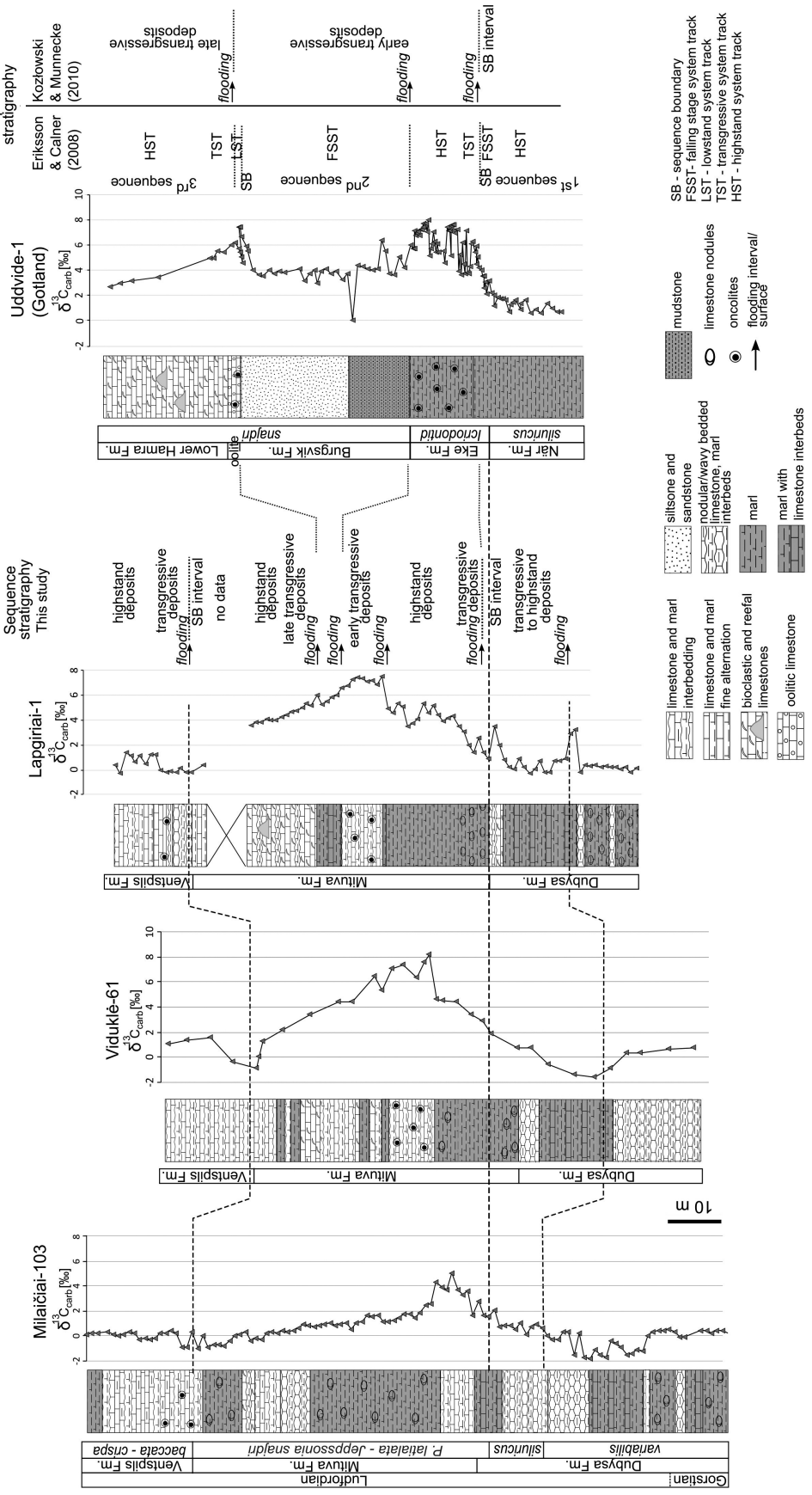

Figure 19. General sedimentary facies and correlation of $\delta^{13}C_{carb}$ and sequence stratigraphy interpretations between Ludfordian sections from Lithuania and Gotland. Data sourced and modified from Martma *et al.* (2005), Eriksson & Calner (2008), Kozlowski & Munnecke (2010), Spiridonov *et al.* (2017b), and Younes *et al.* (2017). The record from Gotland is compositional, *i.e.* compiled from core and outcrop dataset (see Younes *et al.* 2017). The lower $\delta^{13}C$ values within the anomaly in the Burgsvik Fm. are interpreted as a facies effect related to carbonate cement (Younes *et al.* 2017).

distinct from the homogenous micrite that forms oncoids indicates that the oncoids have a different provenance. Conversely, the homogeneous micrite of the mud lithoclasts within the matrix points to the same source material as the oncoids. Furthermore, the close occurrence and often aligned orientation of the mud lithoclasts relative to the oncoids may imply that the oncoids underwent abrasion during transport due to incomplete lithification and erosion of semi-lithified carbonate mud (Fig. 6). The diverse fauna observed in the nuclei of oncoids suggests their origin was in open marine conditions of shallow water settings. The presence of cyanobacteria, which played a significant role in constructing the micritic laminae of the cortex, also suggests relatively shallow water environments, because cyanobacteria are photoautotrophs, which occupy subaqueous settings within the photic zone (Pratt 2001). Oncoids probably formed by multi-stage growth involving a period favouring cyanobacterial growth, interrupted by phases of organism encrustation and incorporation of bioclast or sediment within the cortex, and times of rolling, thereby implying a certain amount of energy. The floatstone texture of oncoid-bearing lithologies supports the interpretation of redeposition of oncoids, which are presumed to have been eroded and transported, likely during storms or through gravity-induced mechanisms from a relatively shallow setting to the deeper muddy site of the ramp. Redeposition of sediments may imply a certain degree of oncoid deformation if not lithified completely. This suggestion could be evidenced in the cloudy appearance of oncoids, *i.e.* non-uniform and irregular forms. Variably-shaped oncoids, resembling oncoids from this study, are also reported from Eke Fm. (Gotland) in Uddvide-1 drill core (Younes 2012). Moreover, oncoids from Gotland described by Eriksson & Calner (2008), Samtleban *et al*. (2000), and Younes (2012) are likewise enclosed within a matrix of argillaceous and micritic limestone and marly matrix, and occur in a similar position on the shelf (proximal platform slope seaward of reef barrier), similarly to the described oncoids in this study.

The abrupt lithology change from marls of the Unit V to crinoidal-bioclastic grainstone-rudstone (Unit VI), accompanied by abundant pyritization of bioclasts points to an erosional boundary (Fig. 7C). A grain-supported texture of the limestone suggests deposition in high energy settings allowing the fine matrix to be winnowed, while the subordinate interbeds of marls points to periodic deposition in relatively calm settings with an influence of marly sedimentation. Hence, the non-reefal bioclastic limestone beds are interpreted as having been deposited within a wave-agitation zone, referring to open marine shallow subtidal depths.

The presence and gradual increase in reef-associated fauna up section suggest proximity, progressive encroachment into the reef environment, evidenced by more massive limestone of floatstone and rudstone texture with large stromatoporoids, corals, and crinoids. The drilling core gives only limited opportunities to investigate the shape, extension, and internal structure of organic bodies, however, the rudstone to floatstone textures of the limestone suggest that most of the large bioclasts were likely washed and spread within a near-shoal area. The stromatoporoid facies resemble SMF 6 or RMF 15 after Flügel (2010), placing those deposits respectively within the platform margin to foreslope in a carbonate platform model or open marine environment of the lower inner ramp in a carbonate ramp model. The abundance of fine-grained material (micrite, clay) in the samples may indicate deposition in sheltered areas or sediment trapping between reef-building fauna. There are many examples within the Silurian basin on the shelf of Baltica characterizing the organic accumulation of reef builders, predominantly involving stromatoporoids, from shallow water environments as biostromes (Kershaw 1994, Samtleben *et al*. 2000, Bičkauskas & Molenaar 2008b, Skompski *et al*. 2008, Łuczyński *et al*. 2009, Jarochowska & Kozłowski 2014). It is thought that Ludlow biostromes from Gotland formed laterally wide bank-like bodies at shallow water depths, where the hydrodynamic boundary at the sea surface determined their growth (Samtleben *et al*. 2000). An insightful analysis of the morphometry of the upper Silurian stromatoporoids was conducted by Łuczyński *et al*. (2009). The study emphasized the concept of fractional segregation as the prevailing process governing the transportation and redeposition of stromatoporoids, while high-energy events were less effective in zones of shoals inhabited by wave-action-resistant biota. Subsequently, the facies of Units V and VI are interpreted to reflect the transition from the upper mid-ramp to the inner ramp.

The sedimentary features observed in Unit VII, including marl-limestone fine alternations, intraclasts, low-abundance and -diversity fauna, fenestral fabrics, and mud cracks, allow for the interpretation of its deposits as peritidal within the inner ramp. Variations in fine laminae geometries and their interlamination are common in shallow marine carbonate environments and muddy inner shelves (Demicco & Hardie 1995). Bioturbation was not strong enough to destroy the overall lamination. Lithoclasts indicate some degree of sediment reworking and traction transport, most likely by waves and currents, a process typical of the shallow subtidal to intertidal zones. The presence of desiccation cracks in the mudstone (Fig. 9C, D) points to subaerial exposure. The low-diversity fauna consisting of large ostracods (belonging probably to the family Leperditicopida) preferentially inhabited very shallow marginal marine environments (Vannier *et al.* 2001) in a protected low-energy environment. The mudstone-wackestone with ostracods (Fig. 9B) corresponds well to ramp microfacies RMF 18, which is common for protected

inner ramp settings (Flügel 2010). However, the greater accumulation of ostracods with common convex-up shell orientation (Fig. 9B) suggests storm-induced deposition. On the other hand, the occurrence of echinoderms, which are strictly stenohaline organisms, as well as conodont particles, still indicates a connection with the open sea (Stickle & Diehl 1987). Thus, light and porous echinoderm debris was likely transported by waves and currents to protected shallow water areas. Therefore, this facies association is interpreted to reflect an episode of the maximum shallowing, reaching intertidal palaeodepths, coupled with more restricted realms, resulting in an impoverishment of the biotic assemblage.

Unit VIII is interpreted as a shallowing-upward cycle, with sedimentation generally below a fair-weather wave base ranging from somewhat deeper subtidal up to peritidal settings. The unit starts with slightly nodular/wavy bedded limestone with increased diversity in the faunal assemblage, clearly distinguishable from the underlying peritidal facies. Shell detritus in the wackestone of this package indicates enhanced bioclast reworking, probably related to a period of transgression over the inner ramp, marking the start of a new depositional sequence. A great portion of micrite, locally nodular to wavy-bedded fabrics with dark marl partings, may suggest a deeper subtidal zone. Local accumulation of coral fragments, which bear traces of transportation, accompanied by oncoids (Fig. 10E), as well as the presence of coquinas (Fig. 10A, D) suggest storm-agitated settings. The improved preservation of bioclasts in wackestone with common bivalves, gastropods, and ostracods up section suggests the establishment of low-energy sedimentation at comparatively shallower water depths. Some degree of restriction is indicated by the occurrence of peloids, evidence of micritization, and microborers attacking the surface of bioclasts, all being common phenomena observed in shallow-marine environments (Flügel 2010). The facies of laminated crinoidal mudstone-wackestone (Fig. 10F, G) is interpreted to be deposited in a somewhat protected environment, where the presence of planar, wavy to cross-laminae and intraclasts indicates the overall low-energy sedimentation, but with intermittent action of waves and currents enabling the delivery of crinoids from open marine settings. The bioclastic mudstone-wackestone with dominant molluscs, ostracods, echinoderms, but also brachiopods, suggests a normal marine, low-energy, shallow subtidal environment. The appearance of massive stromatoporoid bioclasts points to stronger water energy (storms), resulting in stromatoporoid dislocation and redeposition to a sheltered zone in close proximity to the reef environment. Thus, Unit VIII reflects a shallowing-upward cycle characterised by a low-energy, normal marine ranging from somewhat deeper to shallow subtidal realms regularly disturbed by storms, with a likely recurrence to somewhat protected environments.

Evolution of depositional environments

The margin of the Baltica in Silurian represents a tropical shallow-water system, where intensity of carbonate production appears to depend largely on water depth (Schlager 2000 and references therein), although sea-bottom morphology and intra-basinal conditions, including temperature, nutrients, salinity, water energy, *etc.*, are also important factors that determine the carbonate factory (summarized in Pomar & Haq 2016). Therefore, with increasing water depth towards offshore shelf settings, the carbonate content decreases, giving way to fine-grained siliciclastic sediments. For a given palaeogeographic location of the studied borehole, the overall shift from marly sedimentation to the carbonate-dominated deposition is observed during the Ludfordian. This change in lithology, therefore, reveals a general long-term shallowing-upward trend. It is important to note that interpreting sequence stratigraphy in a single borehole is much less reliable than interpreting it on a basin scale (Schlager 2002). Besides global sea level changes, the tectonic setting and evolution of the basin, which was subjected to intensive subsidence and high sedimentation rates in the late Silurian, is another factor influencing deposition. Nevertheless, we propose a tentative interpretation of system tracks based on facies characteristics (Figs 3, 19).

The lower part of the studied core section, characterised by background $\delta^{13}C_{carb}$ values in *K. variabilis–P. siluricus* Zones, represents sedimentation within a distal-ramp zone. Unit II is distinguished by its distinct sedimentary features, namely the relative paucity of fossils and the presence of a rhythmic pattern of elongated planar nodules/carbonate beds (Fig. 4B, C). The core interval between ~ 1116 m (here inferred hardground and flooding surface, that corresponds to a small $\delta^{13}C_{carb}$ anomaly, Figs 3, 4B) and 1084 m is marked by a very low yield of conodont elements. This suggests peculiar marine environmental conditions that may have significantly stressed marine ecosystems and individual taxonomic groups. The deepening of the environment could be associated with stagnant and anoxic bottom-water conditions. However, if oxygen-depleted conditions are a likely component mechanism causing Mid-Ludfordian faunal extinctions, it is a matter of ongoing discussion. Geochemical and sedimentary analyses throughout the Mid-Ludfordian interval, mostly carried out on deep-water sedimentary successions, revealed the presence of anoxic to even euxinic water masses (*e.g.* Kozłowski 2015; Bowman *et al*. 2019, 2020; Frýda *et al*. 2021a; del Rey *et al*. 2023), but these analyses did not definitively establish the cause of extinction, as poor oxygenation is generally common in deep-water settings, as already noted by Claussen & Munnecke (2024).

The greater content, diversity, and frequency of occurrence of bioclastic material towards the top of Unit III

reflect a gradual transition to mid-ramp settings. This interval is marked by the rising limb of the $\delta^{13}C_{carb}$ (Fig. 3) and the lower half of the *P. latialata–Jeppssonia snajdri* Interval Biozone. An increased content of skeletal grains and overall carbonate content (see progressive decline in gamma-ray values, Fig. 3) demonstrates the proximity to the carbonate factory. Most of Unit III appears to have been deposited during highstand conditions, involving depositional regression and progradation (Schlager 2002). Storm activity, as a mechanism of grain transport from shallow to deeper water settings, is particularly pronounced in the middle ramp (*e.g.* Tucker & Wright 1990, Burchette & Wright 1992, Flügel 2010). Here, an issue worth discussion is the nature of a 2-metre thick limestone at the top of Unit II characterised by intercalations of thin beds of skeletal limestone (Fig. 3, 5B, C), coinciding with the onset of the CIE. The lower boundary of limestone with the underlying marl of Unit II is sharp. The bioclastic grainstone and packstone beds have diagnostic importance in the interpretation of depositional settings. The grain-supported texture suggests allochthonous sedimentation, likely storm-induced (proximal tempestites), or washed in/reworked deposition within the middle ramp. Bioclastic components in those sediments indicate that they were sourced from shoal-proximal settings. Storm-related deposits are frequent elements in shallowing-upward sequences (Flügel 2010), like in Upper Muschelkalk strata of the Middle Triassic that represent deposits of a storm-dominated carbonate ramp (Adams & Diamond 2019). Downstepping shoal-water deposits on the slope are characteristic of lowstand conditions (Schlager 2002, Catuneanu *et al*. 2011). The sharp lithology change suggests an abrupt shift from outer to mid-ramp conditions, potentially reflecting regression, with the unconformity representing a significant hiatus in eastern Lithuania (Fig. 2). Therefore, this limestone interval present at Unit II and III transition is considered as a sequence boundary (SB) interval (Fig. 3). Correlatively, at a similar stratigraphic level (interval encompassing *siluricus* Zone–*P. latialata–Jeppssonia snajdri* Interval Biozone boundary), prolonged exposure of the carbonate platform was determined at the transition between Isakivtsy and Prygorodok Fms in Podolia, Ukraine (Jarochowska & Kozłowski 2014), hiatuses and a missing $\delta^{13}C$ excursions were determined in Ohesaare core from Estonia (marginal part of the Baltic Basin, Kaljo *et al*. 2022) and in the Pozary and Muslovka Quarries (shallow part of the Prague Basin, Slavík *et al*. 2010, Gocke *et al*. 2013). Likewise, abrupt facies shift from deep to shallower waters in the Holy Cross Mountains (Kozłowski 2003, Kozłowski & Munnecke 2010), and Gotland (Calner *et al*. 2004, Eriksson & Calner 2008, Younes *et al.* 2017) – all marginal Baltic Basin settings – have been interpreted as rapid shallowing associated with hiatuses. Falling-stage systems tracts, beginning near the *Kozłowskii* extinction level and followed by lowstand, are also recorded in deeper sections (Mielnik-1 borehole, Poland, Kozłowski & Sobień 2012). Collectively, these examples support a consensus: sea-level fall likely preceded the CIE. Global sea-level reconstructions for the Silurian, stated by Johnson (2006) and Haq & Schutter (2008), and compared at the same time scale (see Johnson 2010), suggest a peak highstand near the *siluricus* and *P. latialata–J. snajdri* zones boundary (Gómez *et al*. 2021), followed by a fall in sea level towards the *crispa* Zone. This timing contradicts sedimentological evidence from the Lapgiriai-1 core and other localities such as Gotland, Poland, and Podolia (as previously discussed and summarized in Munnecke *et al*. 2010), where sea-level decline in the late *siluricus* Zone and low sea level persisted through the *Icriodontid* Zone (*sensu* Jeppsson 2005, Eriksson & Calner 2008).

The interval of increased gamma-ray values at the beginning of Unit III marks a transgressive phase with renewed marly deposition, followed by highstand conditions, as noted above. The interpretation of skeletal limestone beds as proximal tempestites is backed by their interbedding within marls (Flügel 2010). This suggests thin, sheet-like accumulations confined to shoal proximity and with limited lateral continuity – an important consideration for hydrocarbon exploration, as seen in Lithuania (Zdanaviciutė & Lazauskienė 2007 and references therein).

Unit IV marks an upward transition within the middle ramp, characterized by the deposition of oncoid-bearing beds. Once again, mud-supported textures indicate relatively quiet-water sedimentation, but the redeposited nature of the oncoids likely implies deposition during storm events or gravity-induced sliding of semi-consolidated fine-grained sediments down a slope. As demonstrated by Kenter (1990), mud-dominated slopes of carbonate platforms, where slump facies are common, are characterized by relatively low slope angles, with a maximum of 15°. This contrasts with grain-supported textures, which may develop on steeper slopes. These findings suggest that mud-dominated facies on the shelf during the Ludfordian could not have formed steeply-angled slopes.

During transgressive phases, carbonate material may commonly be exported from the shallow shelf areas (Catuneanu *et al*. 2011). The oncoid-rich lithologies could therefore be considered early transgressive deposits. Flooding of the inner ramp zone may enhance tidal currents and wave action, conditions favourable for non-skeletal grains formation (Schlager 2002, Flügel 2010). Therefore, redeposited oncoids are often associated with facies developed during platform flooding (Schlager 2002, Whalen *et al*. 2002, Flügel 2010 and references therein). Alternatively, these oncoidal facies may have formed

during an extended highstand that commenced during the time of Unit III deposition.

The other significant feature of oncoids and other microbialites is their coincidence with maximum values of $\delta^{13}C$ anomaly (our study, Munnecke *et al*. 2003 and summary in Calner 2008) and occurrence within an interval of recovery after mass extinctions, such as the Lau Event (Calner 2005) or the Frasnian-Famennian mass extinction (Whalen *et al*. 2002). An increase in microbially-mediated facies was broadly linked to low biotic diversity (Calner 2005, Riding & Liang 2005) and an elevated seawater saturation state, a critical factor in synsedimentary lithification, that in turn, is essential for the growth and preservation of microbial carbonates (Riding & Liang 2005). Carbonate supersaturation was also considered by Kozłowski (2015) as a driving mechanism for the Mid-Ludfordian CIE.

A distinct reduction in water energy is recorded in a several-metre-thick marly interval of Unit V, which likely indicates a rising sea level (Figs 3, 19). The nature of the surface between Units V and VI is ambiguous (Fig. 7C) and is tentatively interpreted here as a flooding surface resulting from a step-rise in the sea level. Transgressive conditions possibly continued and transitioned to highstand within Unit VI, resulting in deposition of bioclastic limestones followed by reefal limestone within the shoal barrier area, where fair weather wave energy was the greatest along the whole ramp system. This phase of sedimentation corresponds to the upper *P. latialata–J. snajdri* Interval Biozone and declining values of $\delta^{13}C_{carb.}$ The mud-dominated lithologies of Unit VII developed as peritidal deposits, with indications of subaerial exposure within inner ramp settings. This facies marks the SB interval, accompanied by a return to background values on $\delta^{13}C_{carb}$ record (Fig. 3). The character of the facies transition from shoal barrier to intertidal zone cannot be resolved due to missing core segments (Fig. 3). Nevertheless, it is plausible to consider those facies as a peritidal cycle, involving seaward progradation of shallower-water environments over deeper-water ones (Tucker & Wright 1990). The beginning of the Ventspils Fm. deposition probably marks the transition to another phase of deepening, thus initial transgression and flooding of the inner ramp, and subsequent shallowing-upward cycle.

The $\delta^{13}C_{carb}$ record in Lapgiriai-1 core is almost identical with the one from Viduklė-61 core, suggesting that they were situated in a similar position on the shelf throughout the Ludfordian. However, both the isotopic record and the facies development in the studied core show differences in relation to the closely-located Milaičiai-103 core (Figs 1, 19), likely due to irregular ramp topography with local high gradients, supporting the notion of a narrow shoal-barrier facies belt.

Aside from the frequently cited sequence stratigraphy interpretation of the Gotland succession by Eriksson & Calner (2008), Kozłowski & Munnecke (2010) proposed an alternative model (Fig. 19). The model by Eriksson & Calner (2008) comprises three depositional sequences, interpreted as representing long-term regression interrupted by minor sea-level fluctuations. In contrast, Kozłowski & Munnecke (2010) suggested a long-term stillstand, marked by several transgressive pulses, following a major regression coinciding with the onset of the CIE (Fig. 19). Similarities in the sedimentary and chemostratigraphic records of the Gotland and the Lapgiriai-1 successions allow tentative correlation between the two. Low values of $\delta^{13}C_{carb}$ within marls of the När Fm. (Hemse Group), a short rising limb of $\delta^{13}C_{carb}$ within the lower Eke Fm., and maximum isotope values within oncolitic beds of the Eke Fm. could be matched with marls of the Dubysa Fm. to marls and oncolitic beds of the Mituva Fm. (Units II to IV, Figs 3, 19). Both intervals include a contrasting facies interval at the onset of the CIE, thought to result from sea regression (Eriksson & Calner 2008, Kozłowski & Munnecke 2010, and this study). However, the Lapgiriai-1 core shows a much more prominently developed rising limb in the $\delta^{13}C_{carb}$ curve, encompassing the lower part of the *P. latialata–J. snajdri* Interval Biozone, interpreted as deposits formed during transgression and subsequent highstand. This interpretation is similar to that of Eriksson & Calner (2008), who also inferred a rise in sea level at the corresponding stratigraphic level. The oncolitic facies of the Eke Fm. are considered as highstand deposits (Eriksson & Calner, 2008), while in the Lapgiriai-1 core, oncoids are interpreted as having been deposited during early transgression, although highstand settings cannot be excluded. In both Gotland succession models, the time interval during which the Eke and Burgsvic Fms were deposited is considered to have followed a major regression in the late *siluricus* Zone and was characterized by relatively low sea level (Eriksson & Calner 2008, Kozłowski & Munnecke 2010). This low sea level could be attributed to global cooling during the mid-Ludfordian glaciation episode as inferred from isotope measurements (Frýda *et al.* 2021b), and linked to a sedimentary gap in the Eastern Lithuanian (Fig. 2), which, in turn, implies a relatively substantial sea-level drop. The marly Unit V, with still relatively high $\delta^{13}C_{carb}$ values, could correspond roughly to the mudstones of the lower Burgsvic Fm. on Gotland (see the unaltered $\delta^{13}C$ curve from Gotland measured on brachiopods in Samtleben *et al.* 2000 or in Kozłowski & Munnecke 2010), while the Burgsvic Sandstone possibly corresponds to the gap between Units V and VI, expressed as an erosional surface (Figs 3, 7C). Nevertheless, contradiction remains: Eriksson & Calner (2008) interpreted the Burgsvik Fm. as regressive deposits (prodelta muds and further pro-

gradation of a fluvial delta complex during a fall in sea level), whereas the marls of Unit V likely represent transgressive deposits (Figs 3, 19). The erosional surface between Units V and VI could be correlated with the top of the Burgsvic Sandstone on Gotland, identified as a sequence boundary in the model of Eriksson & Calner (2008), followed by a transgressive system track of the third sequence (Fig. 19). Kozłowski & Munnecke (2010), meanwhile, interpreted it as a successive flooding surface during the transgressive-punctuated stillstand (Fig. 19). The similar $\delta^{13}C_{carb}$ signature (gradually decreasing values) and system tracks (transgressive and highstand) of the upper portion of the Mituva Fm. (Unit VI) and the Hamra Fm. on Gotland probably indicate synchronous sedimentation. Kozłowski & Munnecke (2010) similarly interpreted the Hamra Fm. as having been deposited during a major post-lowstand sea-level rise (Fig. 19). Thus, although there are observable similarities in sedimentary and chemostratigraphy records between the Lapgiriai-1 and the Gotland sections, which can be roughly correlated, the interpretation of sequence stratigraphy differs in some respects. It is most likely that a combination of several factors, including global sea-level changes, continuous basin subsidence and infill, and a particular stacking pattern, resulted in a dominant long-term progradational trend during the Ludfordian, as previously suggested by Jarochowska & Kozłowski (2014).

Conclusions

Based upon an integrated analysis of the facies, carbon isotope distribution, and conodont ranges and abundances along the Ludfordian section deposited at the shelf of Baltica (Central Lithuania), the following conclusions can be drawn:

(1) The succession spans the *K. variabilis* to *J. crispa* conodont Zones, and the recorded positive $\delta^{13}C_{carb}$ excursion reaches values of up to +7.5‰, which is known as the Mid-Ludfordian Carbon Isotope Excursion. This event commences in the uppermost *P. siluricus* and extends throughout the *P. latialata–Jeppssonia snajdri* Interval Biozone. The section is devoid of graptolites, *e.g.* the only species of graptolite *Pristiograptus dubius frequens* Jaekel was found in a marly interval just preceding the onset of the $\delta^{13}C_{carb}$ excursion.

(2) The gradual change from marly facies to carbonate-dominated sedimentation, observed in the upward lithological sequence, reflects a general shallowing-upward trend and a transition from a low-energy distal, deep-water ramp to a low-energy peritidal zone within the inner ramp, interrupted by a high-energy shallow subtidal shoal barrier belt. This transition is the result of a long-term progradational trend, driven by a number of factors, including relative sea-level change, specific sedimentary stacking patterns, and progressive basin subsidence and infilling.

The sedimentological record in the Lapgiriai-1 core suggests a change in water depth during deposition, from distal to mid-ramp settings, at a stratigraphic level coinciding with the onset of CIE. This could be linked to a regression caused by an episode of global cooling. This interpretation is consistent with sedimentological evidences from other locations on different palaeocontinents. Following the regression, sea level rose and developed into a highstand during the time of the increasing $\delta^{13}C_{carb}$ limb. Oncolitic beds, marked by the highest amplitude of $\delta^{13}C_{carb}$ record, are considered to be early transgressive deposits, however, prolonged highstand conditions during their deposition cannot be ruled out. Bioclastic and reefal limestones, which recorded declining $\delta^{13}C_{carb}$ values, reflect a progressive rise in sea level and following highstand. The return to background $\delta^{13}C_{carb}$ level coincides with a new transgression, beginning a new depositional cycle.

Acknowledgements

This project has received funding from the Research Council of Lithuania (LMTLT), agreement No. S-MIP-22-49. Anna Cichon-Pupienis was supported by funding from the Research Council of Lithuania (LMTLT), agreement No. P-MIP-23-129. Andrej Spiridonov, R. Stankevič and S. Radzevičius were supported by the action programme "CA23124 – Social, biological and climatic impacts of salt ages (SaltAges)".

References

Adams, A. & Diamond, L.W. 2019. Facies and depositional environments of the upper Muschelkalk (Schinznach Formation, Middle Triassic) in northern Switzerland. *Swiss Journal of Geosciences 112(2)*, 357–381.
DOI 10.1007/s00015-019-00340-7

Andrew, A.S., Hamilton, P.J., Mawson, R., Talent, J.A. & Whitford, D.J. 1994. Isotopic correlation tools in the mid-Palaeozoic and their relation to extinction events. *The APPEA Journal 34(1)*, 268–278.
DOI 10.1071/AJ93025

Baarli, B.G., Markes, E.J. & Antoshkina, A. 2003. Silurian stratigraphy and paleogeography of Baltica, 3–34. *In* Landing, E. & Johnson, M.E. (eds) *Silurian lands and seas. Paleogeography outside of Laurentia*. *New York State Museum Bulletin 493.*

Barrick, J.E., Kleffner, M.A., Gibson, M.A., Peavey, F.N. & Karlsson, H.R. 2010. The mid-Ludfordian Lau Event and carbon isotope excursion (Ludlow, Silurian) in southern

Laurentia–preliminary results. *Bollettino della Società Paleontologica Italiana 49(1)*, 13–33.

Barrick, J.E., Klapper, G., Kleffner, M.A. & Karlsson, H.R. 2011. Conodont biostratigraphy and stable isotope chemostratigraphy of the lower Henryhouse Formation (Gorstian-early Ludfordian, Ludlow, Silurian), southern Oklahoma, USA. *Memoirs of the Association of Australasian Palaeontologists 39*, 51–70.

Barrick, J.E., Klapper, G. & Peavey, F.N. 2024. Conodont biostratigraphy of the upper member of the Henryhouse Formation (late Ludfordian-Prídolí, Silurian), southern Oklahoma, USA. *Stratigraphy 21(4)*, 287–322. DOI 10.29041/strat.21.4.02

Bassett, M.G., Kaljo, D. & Teller, L. 1989. The Baltic region, 158–170. *In* Holland, C. & Bassett, M.G. (eds) *A Global Standard for the Silurian System*. 325 pp. National Museum of Wales Geological Series, Cardiff.

Bičkauskas, G. & Molenaar, N. 2008a. Facies and depositional environment of the Pridoli carbonate ramp in the Silurian Baltic Basin, Lithuania. *Geologija 50*, 264–274. DOI 10.2478/v10056-008-0052-z

Bičkauskas, G. & Molenaar, N. 2008b. The nature of the so-called 'reefs' in the Pridolian carbonate system of the Silurian Baltic basin. *Geologija 50*, 94–104. DOI 10.2478/v10056-008-0013-6

Bowman, C.N., Young, S.A., Kaljo, D., Eriksson, M.E., Them, T.R., Hints, O., Martma, T. & Owens, J.D. 2019. Linking the progressive expansion of reducing conditions to a stepwise mass extinction event in the late Silurian oceans. *Geology 47(10)*, 968–972. DOI 10.1130/G46571.1

Bowman, C.N., Lindskog, A., Kozik, N.P., Richbourg, C.G., Owens, J.D. & Young, S.A. 2020. Integrated sedimentary, biotic, and paleoredox dynamics from multiple localities in southern Laurentia during the late Silurian (Ludfordian) extinction event. *Palaeogeography, Palaeoclimatology, Palaeoecology 553*, 109799. DOI 10.1016/j.palaeo.2020.109799

Branson, E.B. & Mehl, M. G. 1933. Conodont studies number 1. Conodonts from the Bainbridge (Silurian) of Missouri. *University of Missouri Studies 8*, 39–52.

Burchette, T.P. & Wright, V.P. 1992. Carbonate ramp depositional systems. *Sedimentary Geology 79(1–4)*, 3–57. DOI 10.1016/0037-0738(92)90003-A

Calner, M. 2005. A Late Silurian extinction event and anachronistic period. *Geology 33(4)*, 305–308. DOI 10.1130/G21185.1

Calner, M. 2008. Silurian global events — at the tipping point of climate change, 21–58. *In* Elewa, A.M.T. (ed.) *Mass Extinctions*. Springer Verlag, Heidelberg. DOI 10.1007/978-3-540-75916-4_4

Calner, M., Jeppsson, L. & Munnecke, A. 2004. The Silurian of Gotland — Part I: Review of the stratigraphic framework, event stratigraphy, and stable carbon and oxygen isotope development. *Erlanger Geologische Abhandlungen, Sonderband 5*, 113–131.

Catuneanu, O., Galloway, W.E., Kendall, C.G.S.C., Miall, A.D., Posamentier, H.W., Strasser, A. & Tucker, M.E. 2011. Sequence stratigraphy: methodology and nomenclature. *Newsletters on Stratigraphy 44*, 173–245. DOI 10.1127/0078-0421/2011/0011

Claussen, A.L. & Munnecke, A. 2024. Benthic response to the strong Silurian climatic fluctuations—implications from Gotland (Sweden). *Facies 70(4)*, 14. DOI 10.1007/s10347-024-00686-x

Cocks, L.R.M. & Torsvik, T.H. 2005. Baltica from the late Precambrian to mid-Palaeozoic times: the gain and loss of a terrane's identity. *Earth-Science Reviews 72(1–2)*, 39–66. DOI 10.1016/j.earscirev.2005.04.001

Cramer, B.D., Brett, C.E., Melchin, M.J., Männik, P., Kleffner, M.A., Mclaughlin, P.I., Loydell, D.K., Munnecke, A., Jeppsson, L. & Corradini, C. 2011. Revised correlation of Silurian Provincial Series of North America with global and regional chronostratigraphic units and $\delta^{13}C_{carb}$ chemostratigraphy. *Lethaia 44*, 185–202. DOI 10.1111/j.1502-3931.2010.00234.x

Demicco, R.V. & Hardie, L.A. 1995. *Sedimentary structures and early diagenetic features of shallow marine carbonate deposits*. 265 pp. SEPM Society for Sedimentary Geology, Tulsa. DOI 10.2110/sepmatl.01.

Eichenseer, K., Balthasar, U., Smart, C.W., Stander, J., Haaga, K.A. & Kiessling, W. 2019. Jurassic shift from abiotic to biotic control on marine ecological success. *Nature Geoscience 12*, 638–642. DOI 10.1038/s41561-019-0392-9

Einasto, R.Z., Abushik, A.F., Kaljo, D.P., Koren', T.N., Modzalevskaya, T.L. & Nestor, H.Z. 1986. Silurian sedimentation and the fauna of the East Baltic and Podolian marginal basins: a comparison, 269–279. *In* Koren', T.N. & Lyarskaya, L.A. (eds) *Theory and Practice of Ecostratigraphy*. Nauka, Leningrad.

Eriksson, M.J. & Calner, M. 2008. A sequence stratigraphical model for the Late Ludfordian (Silurian) of Gotland, Sweden: implications for timing between changes in sea level, palaeoecology, and the global carbon cycle. *Facies 54*, 253–276. DOI 10.1007/s10347-007-0128-y

Flügel, E. 2010. *Microfacies of Carbonate Rocks: Analysis, Interpretation and Application. 2nd ed*. 984 pp. Springer, Berlin & Heidelberg. DOI 10.1007/978-3-642-03796-2

Frýda, J. & Manda, Š. 2013. A long-lasting steady period of isotopically heavy carbon in the late Silurian ocean: evolution of the $\delta^{13}C$ record and its significance for an integrated $\delta^{13}C$, graptolite and conodont stratigraphy. *Bulletin of Geosciences 88*, 463–482. DOI 10.3140/bull.geosci.1436

Frýda, J., Lehnert, O., Frýdová, B., Farkaš, J. & Kubajko, M. 2021a. Carbon and sulfur cycling during the mid-Ludfordian anomaly and the linkage with the late Silurian Lau/Kozlowskii Bioevent. *Palaeogeography, Palaeoclimatology, Palaeoecology 564*, 110152. DOI 10.1016/j.palaeo.2020.110152

Frýda, J., Lehnert, O., Joachimski, M., Männik, P., Kubajko, M., Mergl, M., Farkaš, J. & Frýdová, B. 2021b. The Mid-Ludfordian (late Silurian) Glaciation: a link with global changes in ocean chemistry and ecosystem overturns. *Earth-Science Reviews 220*, 1–32. DOI 10.1016/j.earscirev.2021.103652

Girard, C. & Renaud, S. 2007. Quantitative conodont-based approaches for correlation of the Late Devonian Kellwasser

anoxic events. *Palaeogeography, Palaeoclimatology, Palaeoecology 250*, 114–125. DOI 10.1016/j.palaeo.2007.03.007

Gocke, M., Lehnert, O. & Frýda, J. 2013. Facies development across the Late Silurian Lau Event based on temperate carbonates of the Prague Basin (Czech Republic). *Facies 59*, 611–630. DOI 10.1007/s10347-012-0328-y

Gómez, M.J., Mestre, A., Corradini, C. & Heredia, S. 2021. A new species, Ozarkodina huenickeni, from the upper Silurian–Lower Devonian in San Juan Precordillera, South America. *Journal of South American Earth Sciences 108*, 103174. DOI 10.1016/j.jsames.2021.103174

Haq, B.U. & Schutter, S.R. 2008. A chronology of Paleozoic sea-level changes. *Science 322*, 64–68. DOI 10.1126/science.1161648

Hladil, J., Vondra, M., Čejchan, P., Vích, R., Koptíková, L. & Slavík, L. 2010. The dynamic time-warping approach to comparison of magnetic-susceptibility logs and application to Lower Devonian calciturbidites (Prague Synform, Bohemian Massif). *Geologica Belgica 13(4)*, 385–406.

Horn, H.S. 1966. Measurement of "overlap" in comparative ecological studies. *The American Naturalist 100*, 419–424. DOI 10.1086/282436

Jarochowska, E. & Kozłowski, W. 2014. Facies development and sequence stratigraphy of the Ludfordian (Upper Silurian) deposits in the Zbruch River Valley, Podolia, western Ukraine: Local facies overprint on the $\delta^{13}C_{carb}$ record of a global stable carbon isotope excursion. *Facies 60(1)*, 347–369. DOI 10.1007/s10347-013-0370-4

Jarochowska, E., Bremer, O., Heidlas, D., Pröpster, S., Vandenbroucke, T.R.A. & Munnecke, A. 2016. End-Wenlock terminal Mulde carbon isotope excursion in Gotland, Sweden: integration of stratigraphy and taphonomy for correlations across restricted facies and specialized faunas. *Palaeogeography, Palaeoclimatology, Palaeoecology 457*, 304–322. DOI 10.1016/j.palaeo.2016.06.031

Jeppsson, L. 1998. Silurian oceanic events: summary of general characteristics, 239–257. *In* Landing, E. & Johnson, J.M. (eds) *Silurian Cycles: Linkages of Dynamic Stratigraphy with Atmospheric, Oceanic and Tectonic Changes. New York State Museum. Bulletin 491*.

Jeppsson, L. 2005. Conodont-based revisions of the Late Ludfordian on Gotland, Sweden. *GFF 127(4)*, 273–282. DOI 10.1080/11035890501274273

Jeppsson, L. & Aldridge, R. 2000. Ludlow (late Silurian) oceanic episodes and events. *Journal of the Geological Society 157*, 1137–1148. DOI 10.1144/jgs.157.6.1137

Jeppsson, L. & Anehus, R. 1995. A buffered formic acid technique for conodont extraction. *Journal of Paleontology 69*, 790–794. DOI 10.1017/S0022336000035319

Jeppsson, L., Talent, J.A., Mawson, R., Andrew, A., Corradini, C., Simpson, A.J., Wigforss-Lange, J. & Schönlaub, H.P. 2012. Late Ludfordian correlations and the Lau Event, 653–675. *In* Talent, J.A. (ed.) *Earth and Life: Global Biodiversity, Extinction Intervals and Biogeographic Perturbations Through Time*. Springer, Netherlands. DOI 10.1007/978-90-481-3428-1_21

Johnson, M.E. 2006. Relationship of Silurian sea-level fluctuations to oceanic episodes and events. *GFF 128(2)*, 115–121. DOI 10.1080/11035890601282115

Johnson, M.E. 2010. Tracking Silurian eustasy: Alignment of empirical evidence or pursuit of deductive reasoning? *Palaeogeography, Palaeoclimatology, Palaeoecology 296(3–4)*, 276–284. DOI 10.1016/j.palaeo.2009.11.024

Kaljo, D., Martma, T., Märss, T., Nestor, V.K. & Viira, V. 2022. A bio- and chemostratigraphic search for the Mid-Ludfordian Carbon Isotope Excursion interval in the Ludlow of the Ohesaare core, Estonia. *Estonian Journal of Earth Sciences 71(1)*, 44–60. DOI 10.3176/earth.2022.04

Kaminskas, D., Michelevičius, D. & Blažauskas, N. 2015. New evidence of an early Pridoli barrier reef in the southern part of the Baltic Silurian basin based on three-dimensional seismic survey, Lithuania. *Estonian Journal of Earth Sciences 64(1)*, 47–55. DOI 10.3176/earth.2015.09

Kenter, J.A. 1990. Carbonate platform flanks: slope angle and sediment fabric. *Sedimentology 37(5)*, 777–794. DOI 10.1111/j.1365-3091.1990.tb01825.x

Kershaw, S. 1994. Classification and geological significance of biostromes. *Facies 31(1)*, 81–91. DOI 10.1007/BF02536934

Klaamann, E. & Einasto, R. 1982. Coral reefs of Baltic Silurian (structure, facies relations), 35–41. *In* Kaljo, D. & Klaamann, E. (eds) *Ecostratigraphy of the East Baltic Silurian*. Valgus, Tallin.

Kozłowski, W. 2003. Age, sedimentary environment and palaeogeographical position of the Late Silurian oolitic beds in the Holy Cross Mountains (Central Poland). *Acta Geologica Polonica 53(4)*, 341–357.

Kozłowski, W. 2015. Eolian dust influx and massive whitings during the Kozlowski/Lau Event: carbonate hypersaturation as a possible driver of the mid-Ludfordian Carbon Isotope Excursion. *Bulletin of Geosciences 90(4)*, 807–840. DOI 10.3140/bull.geosci.1581

Kozłowski, W. 2020. Marine snow and epipelagic suspensoids in the Reda carbonates and a pronounced mid-Ludfordian (Silurian) CIE in the axis of the Baltic Basin (Poland). *Acta Geologica Polonica 70(4)*, 529–567. DOI 10.24425/agp.2020.132262

Kozłowski, W. & Munnecke, A. 2010. Stable carbon isotope development and sea-level changes during the Late Ludlow (Silurian) of the Łysogóry region (Rzepin section, Holy Cross Mountains, Poland). *Facies 56*, 615–633. DOI 10.1007/s10347-010-0220-6

Kozłowski, W. & Sobień, K. 2012. Mid-Ludfordian coeval carbon isotope, natural gamma ray and magnetic susceptibility excursions in the Mielnik IG-1 borehole (Eastern Poland) – dustiness as a possible link between global climate and the Silurian carbon isotope record. *Palaeogeography, Palaeoclimatology, Palaeoecology 339*, 74–97. DOI 10.1016/j.palaeo.2012.04.024

Lazauskienė, J., Stephenson, R., Šliaupa, S. & Van Wees, J.D. 2002. 3-D flexural modelling of the Silurian Baltic Basin. *Tectonophysics 346(1–2)*, 115–135. DOI 10.1016/S0040-1951(01)00231-1

Lehnert, O., Eriksson, M.E., Calner, M., Joachimski, M. & Buggisch, W. 2007a. Concurrent sedimentary and isotopic indications for global climatic cooling in the Late Silurian. *Gŭshēngwùxué Bào 46*, 249–255.

Lehnert, O., Fryda, J., Buggisch, W., Manda, S., Ortega, G. & Aceñolaza, G.F. 2003. A first report of the Ludlow Lau event from the Prague Basin (Barrandian, Czech Republic), 139–144. *In* Ortega, G. & Aceñolaza, G.F. (eds) *Proceedings of the 7th International Graptolite Conference & Field Meeting of the International Subcommission on Silurian Stratigraphy. Serie Correlación Geológica 18.*

Lehnert, O., Frýda, J., Buggisch, W., Munnecke, A., Nützel, A., Kříž, J. & Manda, Š. 2007b. $\delta^{13}C$ record across the Ludlow Lau Event: new data from mid palaeolatitudes of northern peri-Gondwana (Prague Basin, Czech Republic). *Palaeogeography, Palaeoclimatology, Palaeoecology 245*, 227–244. DOI 10.1016/j.palaeo.2006.02.022

Lovejoy, S. & Spiridonov, A. 2024. The Fractional Macro-Evolution Model: a simple quantitative scaling macroevolution model. *Paleobiology 50(2)*, 1–25. DOI 10.1017/pab.2023.38

Loydell, D.K. & Frýda, J. 2011. At what stratigraphical level is the mid-Ludfordian (Ludlow, Silurian) positive carbon isotope excursion in the type Ludlow area, Shropshire, England. *Bulletin of Geosciences 86(2)*, 197–208. DOI 10.3140/bull.geosci.1257

Łuczyński, P., Skompski, S. & Kozłowski, W. 2009. Sedimentary history of Upper Silurian biostromes of Podolia (Ukraine) based on stromatoporoid morphometry. *Palaeogeography, Palaeoclimatology, Palaeoecology 271*, 225–239. DOI 10.1016/j.palaeo.2008.10.017

Łuczyński, P., Kozłowski, W. & Skompski, S. 2015. Regressive–transgressive cyclothem with facies record of the re-flooding window in the Late Silurian carbonate succession (Podolia, Ukraine). *Acta Geologica Polonica 65(3)*, 297–318. DOI 10.1515/agp-2015-0013

Machel, H.G. & Hunter, I.G. 1994. Facies models for Middle to Late Devonian shallow-marine carbonates, with comparisons to modern reefs: a guide for facies analysis. *Facies 30*, 155–176. DOI 10.1007/BF02536895

Martma, T., Brazauskas, A., Kaljo, D., Kaminskas, D. & Musteikis, P. 2005. The Wenlock–Ludlow carbon isotope trend in the Vidukle core, Lithuania, and its relations with oceanic events. *Geological Quarterly 49(2)*, 223–234.

Marwan, N. & Webber, C.L. Jr. 2015. Mathematical and computational foundations of recurrence quantifications, 3–43. *In* Webber, C.L. Jr. & Marwan, N. (eds) *Recurrence Quantification Analysis – Theory and Best Practises*. Springer. DOI 10.1007/978-3-319-07155-8_1

Marwan, N., Thiel, M. & Nowaczyk, N.R. 2002. Cross recurrence plot based synchronization of time series. *Nonlinear Processes in Geophysics 9*, 325–331. DOI 10.5194/npg-9-325-2002

Marwan, N., Romano, M.C., Thiel, M. & Kurths, J. 2007. Recurrence plots for the analysis of complex systems. *Physics Reports 438*, 237–329. DOI 10.1016/j.physrep.2006.11.001

Marwan, N., Donges, J.F., Donner, R.V. & Eroglu, D. 2021. Nonlinear time series analysis of palaeoclimate proxy records. *Quaternary Science Reviews 274*, 107245. DOI 10.1016/j.quascirev.2021.107245

Mathes, G.H., Van Dijk, J., Kiessling, W. & Steinbauer, M.J. 2021. Extinction risk controlled by interaction of long-term and short-term climate change. *Nature Ecology & Evolution 5*, 304–310. DOI 10.1038/s41559-020-01377-w

Melchin, M.J., Sadler, P.M. & Cramer, B.D. 2020. The Silurian Period, 695–732. *In* Gradstein, F.M., Ogg, J.G., Schmitz, M.D. & Ogg, G.M. (eds) *Geologic Time Scale 2020*. Elsevier. DOI 10.1016/B978-0-12-824360-2.00021-8

Mergl, M., Frýda, J. & Kubajko, M. 2018. Response of organophosphatic brachiopods to the mid-Ludfordian (late Silurian) carbon isotope excursion and associated extinction events in the Prague Basin (Czech Republic). *Bulletin of Geosciences 93(3)*, 369–400. DOI 10.3140/bull.geosci.1710

Miller, C.G. & Aldridge, R.J. 1997. Ozarkodina remscheidensis plexus conodonts from the upper Ludlow (Silurian) of the Welsh Borderland and Wales. *Journal of Micropalaeontology 16(1)*, 41–49. DOI 10.1144/jm.16.1.41

Munnecke, A., Calner, M., Harper, D.A.T. & Servais, T. 2010. Ordovician and Silurian sea-water chemistry, sea level, and climate: a synopsis. *Palaeogeography, Palaeoclimatology, Palaeoecology 296(3–4)*, 389–413. DOI 10.1016/j.palaeo.2010.08.001

Munnecke, A., Samtleben, C. & Bickert, T. 2003. The Ireviken event in the Lower Silurian of Gotland, Sweden – relation to similar Palaeozoic and Proterozoic events. *Palaeogeography, Palaeoclimatology, Palaeoecology 195*, 99–124. DOI 10.1016/S0031-0182(03)00304-3

Nehring-Lefeld, M., Modliński, Z. & Swadowska, E. 1997. Thermal evolution of the Ordovician in the western margin of the East-European Platform: CAI and Ro data. *Geological Quarterly 41(2)*, 129–138.

Pander, C.H. 1856. *Monographie der fossilen Fische des Silurischen Systems der Russisch Baltischen Gouvernements*. 79 pp. Buchdruckerei der Kaiserlichen Akademie der Wissenschafen, St. Petersburg.

Paškevičius, J. 1997. *The Geology of the Baltic States*. 387 pp. Geological Survey of Lithuania, Vilnius.

Paškevičius, J., Lapinskas, P., Brazauskas, A., Musteikis, P. & Jacyna, J. 1994. Stratigraphic revision of the regional stages of the Upper Silurian part in the Baltic Basin. *Geologija (Vilnius) 17*, 64–87.

Philip, G.M. 1965. Lower Devonian conodonts from the Tyers area, Gippsland, Victoria. *Proceedings of the Royal Society of Victoria 79(1)*, 95–115.

Pomar, L. & Haq, B.U. 2016. Decoding depositional sequences in carbonate systems: concepts vs experience. *Global and Planetary Change 146*, 190–225. DOI 10.1016/j.gloplacha.2016.10.001

Pratt, B.R. 2001. Calcification of cyanobacterial filaments: Girvanella and the origin of lower Paleozoic lime mud. *Geology 29(9)*, 763–766. DOI 10.1130/0091-7613(2001)029<0763:COCFGA>2.0.CO;2

Radzevičius, S., Spiridonov, A. & Brazauskas, A. 2014a. Application of wavelets to the cyclostratigraphy of the Upper

Homerian (Silurian) Gėluva Regional Stage in the Viduklė-61 deep well (Western Lithuania), 437–440. *In* Pais, J. (ed.) *STRATI 2013*. Springer, Berlin. DOI 10.1007/978-3-319-04364-7_84

Radzevičius, S., Spiridonov, A. & Brazauskas, A. 2014b. Integrated middle–upper Homerian (Silurian) stratigraphy of the Viduklė-61 well, Lithuania. *GFF 136*, 218–222. DOI 10.1080/11035897.2013.866976

Radzevičius, S., Spiridonov, A., Brazauskas, A., Norkus, A., Meidla, T. & Ainsaar, L. 2014c. Upper Wenlock $\delta^{13}C$ chemostratigraphy, conodont biostratigraphy and palaeoecological dynamics in the Ledai-179 drill core (Eastern Lithuania). *Estonian Journal of Earth Sciences 63*, 293–299. DOI 10.3176/earth.2014.33

Radzevičius, S., Spiridonov, A., Brazauskas, A., Dankina, D., Rimkus, A., Bičkauskas, G., Kaminskas, D., Meidla, T. & Ainsaar, L. 2016. Integrated stratigraphy, conodont turnover and paleoenvironments of the Upper Wenlock and Ludlow of the Vilkaviškis-134 core (Lithuania). *Newsletters on Stratigraphy 49(2)*, 321–336. DOI 10.1127/nos/2016/0074

Radzevičius, S., Tumakovaitė, B. & Spiridonov, A. 2017. Upper Homerian (Silurian) high-resolution correlation using cyclostratigraphy: an example from Western Lithuania. *Acta Geologica Polonica 67*, 307–322. DOI 10.1515/agp-2017-0011

Radzevičius, S., Stankevič, R., Budginas, R., Cichon-Pupienis, A., Venckutė-Aleksienė, A., Meidla, T., Ainsaar, L. & Spiridonov, A. 2023. Integrated stratigraphy of the Ludlow (Silurian) of the Baubliai-2 core (western Lithuania) and the record of $\delta^{18}O$ and $\delta^{13}C$ climatically driven co-variability. *Newsletters on Stratigraphy 56(1)*, 75–88. DOI 10.1127/nos/2022/0712

Rey, Á. del, Frýda, J., Calner, M., Frýdová, B., Zhang, F., Wang, C., Planavsky, N. & Dahl, T.W. 2023. Mid-Ludfordian uranium isotope records distinguish the role of expansive marine anoxia in global carbon cycle dynamics during the late Silurian Lau/Kozlowskii bioevent. *Global and Planetary Change 229*, 104248. DOI 10.1016/j.gloplacha.2023.104248

Rhodes, F.H.T. 1953. Some British lower Palaeozoic conodont faunas. *Philosophical Transactions of the Royal Society of London. Series B, Biological Sciences 237(647)*, 261–334. DOI 10.1098/rstb.1953.0005

Riding, R. & Liang, L. 2005. Geobiology of microbial carbonates: metazoan and seawater saturation state influences on secular trends during the Phanerozoic. *Palaeogeography, Palaeoclimatology, Palaeoecology 219(1–2)*, 101–115. DOI 10.1016/j.palaeo.2004.11.018

Sadler, P.M. 2004. Quantitative biostratigraphy – achieving finer resolution in global correlation. *Annual Review of Earth and Planetary Sciences 32*, 187–213. DOI 10.1146/annurev.earth.32.101802.120428

Sadler, P.M. 2012. Integrating carbon isotope excursions into automated stratigraphic correlation: an example from the Silurian of Baltica. *Bulletin of Geosciences 87*, 681–694. DOI 10.3140/bull.geosci.1307

Sadler, P.M., Cooper, R.A. & Crampton, J.S. 2014. High-resolution geobiologic time-lines: progress and potential, fifty years after the advent of graphic correlation. *The Sedimentary Record 12*, 4–9. DOI 10.2110/sedred.2014.3.4

Saltzman, M.R. 2001. Silurian $\delta^{13}C$ stratigraphy: a view from North America. *Geology 29(8)*, 671–674. DOI 10.1130/0091-7613(2001)029<0671:SCSAVF>2.0.CO;2

Samtleben, C., Munnecke, A., Bickert, T. & Pätzold, J. 1996. The Silurian of Gotland (Sweden): facies interpretation based on stable isotopes in brachiopod shells. *Geologische Rundschau 85*, 278–292. DOI 10.1007/s005310050074

Samtleben, C., Munnecke, A. & Bickert, T. 2000. Development of facies and C/O-isotopes in transects through the Ludlow of Gotland: evidence for global and local influences on a shallow-marine environment. *Facies 43*, 1–38. DOI 10.1007/BF02536983

Schlager, W. 2000. Sedimentation rates and growth potential of tropical, cool-water and mud-mound carbonate systems. *Geological Society London, Special Publication 178(1)*, 217–227. DOI 10.1144/GSL.SP.2000.178.01.14

Schlager, W. 2002. *Sedimentology and sequence stratigraphy of carbonate rocks.* 146 pp. Frije Universiteit, Amsterdam.

Skompski, S., Łuczyński, P., Drygant, D. & Kozłowski, W. 2008. High-energy sedimentary events in lagoonal successions of the Upper Silurian of Podolia, Ukraine. *Facies 54*, 277–296. DOI 10.1007/s10347-007-0133-1

Slavík, L., Kříž, J. & Carls, P. 2010. Reflection of the mid-Ludfordian Lau Event in conodont faunas of Bohemia. *Bulletin of Geosciences 85(3)*, 395–414. DOI 10.3140/bull.geosci.1204

Spiridonov, A. 2017. Recurrence and cross recurrence plots reveal the onset of the Mulde Event (Silurian) in the abundance data for Baltic conodonts. *The Journal of Geology 125*, 381–398. DOI 10.1086/691184

Spiridonov, A. & Lovejoy, S. 2022. Life rather than climate influences diversity at scales greater than 40 million years. *Nature 607*, 307–312. DOI 10.1038/s41586-022-04867-y

Spiridonov, A., Brazauskas, A. & Radzevičius, S. 2015. The role of temporal abundance structure and habitat preferences in the survival of conodonts during the mid–early Silurian Ireviken mass extinction event. *PLoS ONE 10*, e0124146 DOI 10.1371/journal.pone.0124146

Spiridonov, A., Brazauskas, A. & Radzevičius, S. 2016. Dynamics of abundance of the mid- to late Pridoli conodonts from the eastern part of the Silurian Baltic Basin: multifractals, state shifts, and oscillations. *American Journal of Science 316*, 363–400. DOI 10.2475/04.2016.03

Spiridonov, A., Kaminskas, D., Brazauskas, A. & Radzevičius, S. 2017a. Time hierarchical analysis of the conodont paleocommunities and environmental change before and during the onset of the lower Silurian Mulde bioevent – a preliminary report. *Global and Planetary Change 157*, 153–164. DOI 10.1016/j.gloplacha.2017.09.002

Spiridonov, A., Stankevič, R., Gečas, T., Šilinskas, T., Brazauskas, A., Meidla, T., Ainsaar, L., Musteikis, P. & Radzevičius, S. 2017b. Integrated record of Ludlow (Upper Silurian) oceanic geobioevents – coordination of changes

in conodont and brachiopod faunas, and stable isotopes. *Gondwana Research 51*, 272–288. DOI 10.1016/j.gr.2017.08.006

Spiridonov, A., Venckutė-Aleksienė, A. & Radzevičius, S. 2017c. Cyst size trends in the genus Leiosphaeridia across the Mulde (lower Silurian) biogeochemical event. *Bulletin of Geosciences 92*, 391–404. DOI 10.3140/bull.geosci.1679

Spiridonov, A., Balakauskas, L., Stankevič, R., Kluczyńska, G., Gedminienė, L. & Stančikaitė, M. 2019. Holocene vegetation patterns in southern Lithuania indicate astronomical forcing on the millennial and centennial time scales. *Scientific Reports 9*, 14711. DOI 10.1038/s41598-019-51321-7

Spiridonov, A., Samsonė, J., Brazauskas, A., Stankevič, R., Meidla, T., Ainsaar, L. & Radzevičius, S. 2020a. Quantifying the community turnover of the uppermost Wenlock and Ludlow (Silurian) conodonts in the Baltic Basin. *Palaeogeography, Palaeoclimatology, Palaeoecology 549*, 109128. DOI 10.1016/j.palaeo.2019.03.029

Spiridonov, A., Stankevič, R., Gečas, T., Brazauskas, A., Kaminskas, D., Musteikis, P., Kaveckas, T., Meidla, T., Bičkauskas, G., Ainsaar, L. & Radzevičius, S. 2020b. Ultra-high resolution multivariate record and multiscale causal analysis of Pridoli (late Silurian): implications for global stratigraphy, turnover events, and climate-biota interactions. *Gondwana Research 86*, 222–249. DOI 10.1016/j.gr.2020.05.015

Spiridonov, A., Vaikutienė, G., Stankevič, R., Druzhinina, O., Šeirienė, V., Subetto, D., Kublitsky, J. & Stančikaitė, M. 2021. Response of freshwater diatoms to cold events in the Late Pleistocene and Early Holocene (SE Baltic region). *Quaternary International 589*, 112–123. DOI 10.1016/j.quaint.2021.02.017

Spiridonov, A., Balakauskas, L. & Lovejoy, S. 2022. Longitudinal expansion fitness of brachiopod genera controlled by the Wilson cycle. *Global and Planetary Change 216*, 103926. DOI 10.1016/j.gloplacha.2022.103926

Stankevič, R., Venckutė-Aleksienė, A., Radzevičius, S. & Spiridonov, A. 2024. Phytoplankton and zooplankton paleocommunity change before and during the onset of the Lau Extinction Event (Ludlow, Silurian). *Marine Micropaleontology 189*, 102368. DOI 10.1016/j.marmicro.2024.102368

Stickle, W.B. & Diehl, W.J. 1987. Effects of salinity on echinoderms. *Echinoderm Studies 2*, 235–285.

Strauss, J.V., Fraser, T.A., Melchin, M.J., Allen, T.J., Malinowski, J.K., Feng, X., Taylor, J.F., Day, J., Gill, B.C. & Sperling, E.A. 2020. The Road River Group of northern Yukon, Canada: early Paleozoic deep-water sedimentation within the Great American Carbonate Bank. *Canadian Journal of Earth Sciences 57(10)*, 1193–1219. DOI 10.1139/cjes-2020-0017

Stricanne, L., Munnecke, A. Pross, J. & Servais, T. 2004. Acritarch distribution along an inshore-offshore transect in the Gorstian (lower Ludlow) of Gotland, Sweden. *Review of Palaeobotany and Palynology 130*, 195–216. DOI 10.1016/j.revpalbo.2003.12.007

Tonarová, P., Frýda, J., Kubajko, M. & Hints, O. 2025. Response of the jawed polychaete fauna to environmental changes during the Mid-Ludfordian (late Silurian) glaciation in the Prague Basin (Czech Republic). *Bulletin of Geosciences 100*, 28 pp. DOI 10.3140/bull.geosci.1913

Torsvik, T.H. & Cocks, L.R.M. 2013. Chapter 2: New global palaeogeographical reconstructions for the Early Palaeozoic and their generation. *Geological Society London, Memoir 38(1)*, 5–24. DOI 10.1144/M38.2

Trauth, M.H., Asrat, A., Duesing, W., Foerster, V., Kraemer, K.H., Marwan, N., Maslin, M.A. & Schaebitz, F. 2019. Classifying past climate change in the Chew Bahir basin, southern Ethiopia, using recurrence quantification analysis. *Climate Dynamics 53*, 2555–2572. DOI 10.1007/s00382-019-04641-3

Tucker, M.E. & Wright, V.P. 1990. *Carbonate Sedimentology*. 496 pp. John Wiley & Sons. DOI 10.1002/9781444314175

Urbanek, A., Radzevičius, S., Kozłowska, A. & Teller, L. 2012. Phyletic evolution and iterative speciation in the persistent Pristiograptus dubius lineage. *Acta Palaeontologica Polonica 57(3)*, 589–611. DOI 10.4202/app.2010.0070

Vannier, J., Wang, S.Q., & Coen, M. 2001. Leperditicopid arthropods (Ordovician–Late Devonian): functional morphology and ecological range. *Journal of Paleontology 75(1)*, 75–95. DOI 10.1666/0022-3360(2001)075<0075:LAOLDF>2.0.CO;2

Vecoli, M., Riboulleau, A. & Versteegh, G.J.M. 2009. Palynology, organic geochemistry and carbon isotope analysis of a latest Ordovician through Silurian clastic succession from borehole Tt1, Ghadamis Basin, southern Tunisia, North Africa: palaeoenvironmental interpretation. *Palaeogeography, Palaeoclimatology, Palaeoecology 273*, 378–394. DOI 10.1016/j.palaeo.2008.05.015

Venckutė-Aleksienė, A., Radzevičius, S. & Spiridonov, A. 2016. Dynamics of phytoplankton in relation to the upper Homerian (Lower Silurian) Lundgreni Event – an example from the Eastern Baltic Basin (Western Lithuania). *Marine Micropaleontology 126*, 31–41. DOI 10.1016/j.marmicro.2016.05.001

Walliser, O.H. 1964. Conodonten des silurs. *Abhandlungen des Hessischen Landesamtes für Bodenforschung 41*, 1–106, Hess. Landesamt f. Bodenforschung.

Webber, C.L. Jr. & Marwan, N. 2015. *Recurrence Quantification Analysis – Theory and Best Practices*. 421 pp. Springer International Publishing. DOI 10.1007/978-3-319-07155-8

Wenzel, B. & Joachimski, M.M. 1996. Carbon and oxygen isotopic composition of Silurian brachiopods (Gotland, Sweden): palaeoceanographic implications. *Palaeogeography, Palaeoclimatology, Palaeoecology 122(1–4)*, 143–166. DOI 10.1016/0031-0182(95)00094-1

Westphal, H. 2006. Limestone-marl alternations as environmental archives and the role of early diagenesis: a critical review. *International Journal of Earth Sciences 95*, 947–961. DOI 10.1007/s00531-006-0084-8

Whalen, M.T., Day, J., Eberli, G.P. & Homewood, P.W. 2002. Microbial carbonates as indicators of environmental change and biotic crises in carbonate systems: examples from the

Late Devonian, Alberta Basin, Canada. *Palaeogeography, Palaeoclimatology, Palaeoecology 181(1–3)*, 127–151. DOI 10.1016/S0031-0182(01)00476-X

Whittingham, M., Spiridonov, A. & Radzevičius, S. 2022. Dynamic ecophenotypy in the Silurian Monograptidae (Graptolithina). *Earth and Environmental Science Transactions of the Royal Society of Edinburgh 113*, 29–38. DOI 10.1017/S1755691021000402

Wilson, J.L. 1975. Carbonate Facies in Geologic History. 471 pp. Springer, New York. DOI 10.1007/978-1-4612-6383-8

Younes, H. 2012. *Carbon isotope chemostratigraphy of the late Silurian Lau Event, Gotland, Sweden*. 44 pp. Master thesis, Lund University, Lund, Sweden.

Younes, H., Calner, M. & Lehnert, O. 2017. The first continuous $\delta^{13}C$ record across the late Silurian Lau Event on Gotland, Sweden. *GFF 139(1)*, 63–69. DOI 10.1080/11035897.2016.1227362

Zdanavičiutė, O. & Lazauskienė, J. 2007. The petroleum potential of the Silurian succession in Lithuania. *Journal of Petroleum Geology 30(4)*, 325–337. DOI 10.1111/j.1747-5457.2007.00325.x

Želvys, T., Brazauskas, A., Spiridonov, A., Balčiūnas, M., Garbaras, A. & Radzevičius, S. 2022. Stable carbon isotope stratigraphy of the Silurian in the Jočionys-299 borehole (eastern Lithuania). Estonian *Journal of Earth Sciences 71(3)*, 127–134. DOI 10.3176/earth.2022.09

Supplementary electronic material

Appendix 1. Conodont occurrences in the Lapgiriai-1 core. The table contains the depths from the surface. Sample mass in g. Total conodont abundance per kg and the numbers of detected conodont elements of each taxon (species) in each sample.

Appendix 2. Stable carbonate carbon and oxygen isotope data of the Lapgiriai-1 core.

Appendix 3. Correlation of carbonate carbon and oxygen isotope data of the Lapgiriai-1 core.